

Manuscript Number: JCOMP-D-17-00772

Title: Second order finite-difference ghost-point multigrid methods for elliptic problems with discontinuous coefficients on an arbitrary interface

Article Type: Regular Article

Keywords: finite-difference method; discontinuous coefficients; ghost-point method; elliptic equation; complex geometry; multigrid

Corresponding Author: Dr. Armando Coco,

Corresponding Author's Institution: Oxford Brookes University

First Author: Armando Coco

Order of Authors: Armando Coco; Giovanni Russo, PhD, Full Professor

Abstract: In this paper we propose a second-order accurate numerical method to solve elliptic problems with discontinuous coefficients in 2D. The method consists of a finite-difference method on a Cartesian grid in which complex geometries (boundaries and interfaces) are embedded. In order to avoid the drop in accuracy caused by the discontinuity of the coefficients across the interface, two numerical values are assigned on grid points that are close to the interface: a real value, that represents the numerical solution on that grid point, and a ghost value, that represents the numerical solution extrapolated from the other side of the interface, obtained by enforcing the assigned non-homogeneous jump conditions on the solution and its flux. The discretization results second order accurate in the solution and its gradient. The linear system arising from the discretization is solved by an efficient multigrid approach. Unlike the 1D case, grid points are not necessarily aligned with the normal derivative and therefore suitable stencils must be chosen to discretize interface conditions in order to achieve second order accuracy in the solution and its gradient. A proper treatment of the interface conditions will allow the multigrid to attain the optimal convergence factor, comparable with the one obtained by Local Fourier Analysis for rectangular domains. The method is robust enough to handle large jump in the coefficients: order of accuracy, monotonicity of the coefficients and good convergence factor are maintained by the scheme.

Suggested Reviewers: Frédéric Gibou PhD

Full Professor, Department of Mechanical Engineering, University of California Santa Barbara  
fgibou@engineering.ucsb.edu

Frédéric Gibou has a wide experience in finite-difference ghost point methods for complex geometries and has published several papers on this topic, ranging from generic elliptic equations or with discontinuous coefficients across an arbitrary interface to more complex Navier Stokes equations, using different methods such as ghost points on Cartesian

grids or adaptive grids, and many others. His knowledge on this field can definitely contribute to provide an effective feedback and improve the final quality of the paper.

Angelo Iollo PhD

Full Professor, Institute de Mathématiques de Bordeaux, Université Bordeaux 1

angelo.iollo@math.u-bordeaux.fr

Angelo Iollo is highly experienced in high performance computing for PDEs in real-life problems, and therefore has published different papers on finite-difference methods for elliptic equations in presence of complex geometries. We are certain he will provide a valuable feedback on the general quality of the paper and on specific aspects, such as discretization accuracy and multigrid.

Stefano Serra-Capizzano PhD

Full Professor, Department of Science and High Technology, Università dell'Insubria

stefano.serrac@uninsubria.it

Stefano Serra-Capizzano has an extensive knowledge and expertise on different areas of Numerical Linear Algebra, including multigrid methods. He can surely provide a valuable review on the multigrid methods proposed in this paper, as well as a qualitative feedback on the discretization method and accuracy analysis.

Martin J Gander PhD

Full Professor, Section de Mathématiques, Université de Genève

Martin.Gander@unige.ch

Martin Gander is very experienced in several fields that are related with some aspects of this paper, such as Domain Decomposition Methods (related with the discretization of the discontinuous coefficient across an irregular interface) and Krylov Subspace Methods (related with the multigrid approach).

## **Second order finite-difference ghost-point multigrid methods for elliptic problems with discontinuous coefficients on an arbitrary interface**

Armando Coco, Giovanni Russo

### *Significance and Novelty*

The paper provides a robust and easy to implement new finite-difference method to numerically solve elliptic equations with discontinuous coefficients.

The significance of the paper can be summarized as follows.

- Elliptic equations with discontinuous coefficients are central to many applications such as steady-state solution of diffusion problems; the Poisson equation arising from the projection method for incompressible two-phase fluids with different physical characteristics; the study of electrostatic phenomena such as those encountered in the simulation of biomolecules' electric potential, and many others.
- The method is implemented in a uniform Cartesian grid, that is notoriously more suitable for parallelization in the High Performance Computing framework, rather than alternative methods such as the class of Finite Element methods.
- Efficient methods for complex geometry are crucial in recent applications, especially if the approach is employed in a time dependent problem with moving geometries/shape morphing. The method proposed in this paper does not overload the total computational cost by re-meshing procedures (that are necessary in concurrent methods, such as Finite Element methods), since the complex geometries are tracked by a level-set function and the boundaries are embedded in a fixed Cartesian uniform grid.
- The method can be extended to the case of adaptive grids (under investigation).

The main novelty of the paper is represented by the following points:

- the accuracy of the discretization is second order not only in the solution but also in the gradient of the solution, in spite of most existing methods, whose solution in the gradient drops to first order of accuracy, as detailed in the introduction section of this paper. This extra accuracy is desirable in many applications, where the computation of the gradient is a crucial step in a more general time-dependent algorithm, such as the incompressible Navier-Stokes equations (the gradient of the pressure is used to enforce the incompressibility condition in the projection method), or the Stefan problem (where the gradient drives the motion of the interface).
- the method can be easily extended in 3D and to higher order of accuracy, provided to enlarge the stencil accordingly;
- second order accuracy in the solution and in the gradient is not influenced by the presence of high jumps in the coefficients;
- the efficiency of the multigrid method is not affected by complex geometries nor by possible high jumps in the coefficient, and it is maintained within an acceptable range around the efficiency predicted in literature by the Local Fourier Analysis for simpler problems (such as rectangular domains and continuous coefficients).

## **Second order finite-difference ghost-point multigrid methods for elliptic problems with discontinuous coefficients on an arbitrary interface**

Armando Coco, Giovanni Russo

### *Research Highlights*

- A finite-difference ghost-point method to solve elliptic equations with discontinuous coefficients in complex geometries is proposed.
- The method is second order accurate in both the solution and its gradient.
- The accuracy is not affected by high jumps in the coefficients.
- A proper geometric multigrid approach is presented, whose efficiency (convergence factor) does not depend on the amplitude of the jump in the coefficient.

# Second order finite-difference ghost-point multigrid methods for elliptic problems with discontinuous coefficients on an arbitrary interface

Armando Coco, Giovanni Russo

May 28, 2017

## Abstract

In this paper we propose a second-order accurate numerical method to solve elliptic problems with discontinuous coefficients in 2D. The method consists of a finite-difference method on a Cartesian grid in which complex geometries (boundaries and interfaces) are embedded, and is second order accurate in the solution and the gradient itself. In order to avoid the drop in accuracy caused by the discontinuity of the coefficients across the interface, two numerical values are assigned on grid points that are close to the interface: a real value, that represents the numerical solution on that grid point, and a ghost value, that represents the numerical solution extrapolated from the other side of the interface, obtained by enforcing the assigned non-homogeneous jump conditions on the solution and its flux. The discretization results second order accurate in the solution and its gradient. The linear system arising from the discretization is solved by an efficient multigrid approach. Unlike the 1D case, grid points are not necessarily aligned with the normal derivative and therefore suitable stencils must be chosen to discretize interface conditions in order to achieve second order accuracy in the solution and its gradient. A proper treatment of the interface conditions will allow the multigrid to attain the optimal convergence factor, comparable with the one obtained by Local Fourier Analysis for rectangular domains. The method is robust enough to handle large jump in the coefficients: order of accuracy, monotonicity of the errors and good convergence factor are maintained by the scheme.

## 1 Introduction

Elliptic equations with discontinuous coefficients arise from the mathematical modelling of a large number of real-life applications. Examples include the steady-state solution of diffusion problems, for instance in the context of solidification processes of materials with different diffusion coefficients across a complex interface [62]; the Poisson equation arising from the projection method for incompressible two-phase fluids with different physical characteristics [58]; the study of electrostatic phenomena such as those encountered in the simulation of biomolecules' electric potential [42], and many more [40, 13]. All these problems may be characterized by complex moving interfaces across which the jump of the solution and its flux must be prescribed for well-posedness. While for interfaces aligned with the grid lines the discretization results straightforward, for complex interfaces it is necessary to adopt a suitable numerical approach.

Among the different approaches that have been proposed to numerically solve this problem, interface-fitted grid methods such as those based on the finite element methods (FEM) [6, 7, 33, 31, 19, 27, 17] are computationally expensive especially for complex moving geometries, since at each time step a new mesh fitting the moving interface must be generated. The computational burden is even more exasperated in three dimensions. This negative aspect is partially alleviated by adopting XFEM methods [16, 35, 24, 37, 29], where the solution space for elements crossed by the interface includes discontinuous functions. For complex moving interfaces a suitable re-meshing procedure still encumber the computational cost, and therefore the problems of this class are most efficiently approached by methods that embed the interface in a fixed Cartesian grid.

The Immersed Boundary Method [51] is a pioneering work for this class of numerical methods, where Peskin proposed a first-order accurate method derived from the discretization of the  $\delta$ -function to model blood flows in the heart.

An extension of [51] to second order accuracy is proposed first by LeVeque and Li in [36] (Immersed Interface Methods), where the authors use a suitable six-point stencil to discretize the elliptic operator in grid points close to the interface and find the coefficients of the stencil by Taylor expansion of the solution. The jump condition of the solution is used to modify the coefficients related to nodes close to the interface in order to attain second-order accuracy overall. Second order accuracy using boundary integral techniques was achieved also by Mayo in [43] to solve Poisson (and biharmonic) equations on complex geometries.

More recently, Fedkiw *et al.* introduced the Ghost-Fluid Method in [22], where the authors solve a two-phase problem with an irregular interface between the two phases. In this method, the values on the grid points on the other side of the interface (*ghost points*) is not the physical value (which refers to the other phase of the problem, leading to a discontinuity in the stencil), but a fictitious value (*ghost value*) found by a continuous extrapolation. The problem is finally reduced to two sub-problems by adopting a multi-domain formulation, and each sub-problem is solved by the same technique adopted to solve a single problem with Dirichlet or Neumann boundary conditions.

Liu *et al.* [41] developed a first-order accurate ghost-fluid method for the elliptic equations in the presence of an irregular interface across which the variable coefficient, the solution and its derivative may have jumps. The discretization of the equation results in a symmetric linear system, thus allowing the use of fast iterative solvers. In the case of Dirichlet boundary conditions, instead of interface jump conditions, a second-order symmetric discretization of the ghost-fluid method is proposed by Gibou *et al.* in [25]. A fourth-order (non-symmetric) version can be found in [26], and several features concerning the ghost-fluid method to solve Poisson problems on complex domains with Dirichlet boundary conditions are detailed in [45].

In [46] the authors studied a simple and efficient method for the Navier-Stokes equations on arbitrary shaped domains. Sharp-edge interface problems are also solved by other techniques such as the matched interface and boundary (MIB) method [63], the finite volume method [48], and the non-symmetric positive definite finite element method [32]. Other methods accounting for complex interfaces are the arbitrary Lagrangian Eulerian method (ALE) [23, 18], the penalization methods [54, 5, 10] and the class of Immersed Finite Volume Methods (IFVM) [21].

Variable high-jump coefficients across the interface have been presented in recent methods, where only numerical tests with jump ratio up to the order of one thousand have been explored [38, 63, 47, 48], although they show some unsolved robustness issues (lack of monotonicity of the error when the grid is refined [38] or accuracy lower than second order [63]). Jump ratios up to one million may occur in some applications, for example in the fluid-structure interaction where the structure is modelled as an extremely high viscosity fluid.

In some applications it is desirable to achieve higher accuracy in the gradient of the solution as well, as for example in the case of the Stefan problem, where the gradient drives the motion of the interface, or in the incompressible Navier-Stokes equations, where the gradient of the pressure is used to enforce the incompressibility condition in the projection method [11, 44]. In [50] Gibou *et al.* propose an efficient finite-volume discretization for Neumann boundary conditions based on cut-cell methods. The method is second-order accurate for the Poisson and heat equation, while it downgrades to first-order accuracy for the Stefan-type problem. In [28] the authors introduce the Voronoi Interface Method to solve elliptic equation with discontinuous coefficients in arbitrary domains. The Cartesian grid is modified close to the interface by adopting a Voronoi mesh in order to discretize straightforwardly normal derivatives. The final linear system arising from the discretization is symmetric positive definite and the accuracy is second order for the solution and first order for the gradient. In [12] the authors introduce additional grid points on the intersections between Cartesian lines and interface to discretize the jump conditions in the solution and its flux adopting a dimension-by-dimension approach, attaining second order accuracy.

Second order accuracy in both the solution and in the gradient is achieved in [15], where we present a ghost-point method to solve elliptic problems in arbitrary domains with mixed (Dirichlet and Neumann) boundary conditions. Some extensions to the case of sharp-edge boundary and variable matrix coefficient is also presented. A suitable geometric multigrid approach is introduced to solve the problem, based on a proper relaxation of the boundary conditions on ghost points, with a relaxation parameter chosen in order to achieve the convergence of the iterative method. The extension of the method for the discontinuous coefficient case in one dimension is presented in [14].

Multigrid method is among the most efficient iterative numerical methods to solve the linear system that arises from the discretization of a class of partial differential equations. Initially designed for elliptic problems, nowadays multigrid methods have been adopted to solve a large variety of problems [8, 59, 30]. Regarding the scope of this paper, namely multigrid for elliptic equations with discontinuous coefficients, a detailed survey can be found in [9]. Several methods have been proposed for the simpler case where the interface is aligned with grid lines. As example, we mention [4, 34], where an operator-dependent interpolation is performed assuming the continuity of the flux (instead of the solution gradient), and [52], where an algebraic multigrid method is proposed based on Galerkin Coarse Grid Operator. For Cartesian grids and arbitrary interfaces, i.e. not aligned with grid lines, we mention the paper [3], where a multigrid approach for solving the linear system arising from the discretization of interface conditions described in [3, 39] is provided. In this multigrid technique a black-box multigrid interpolation is used for grid points away from the interface, while the interpolation weights for grid points near the interface are derived from a Taylor expansion (with a change of coordinates). In [1] this multigrid has been improved by modifying the interpolation and restriction operators in such a way the coarse-grid matrices are M-matrices. A comparison of both geometric multigrid methods [3, 1] with Algebraic Multigrid solvers is performed in [2] for the underlying discretization, showing that the multigrid in [1] is the most efficient. Other recent developments of multigrid solvers for non-smooth coefficients can be found in [60], where a geometric multigrid method for multiple interfaces in higher dimensions is proposed, where an accurate interpolation captures the correct boundary conditions at the interfaces via a level set function, and the issues coming from the storage of the coarse-grid matrix are avoided. In [61] the coarse grid points are selected in such a way the irregular interfaces are resolved as much as possible: only linear interpolation is needed to obtain fast convergence.

In this paper, the method proposed in [15] for continuous coefficients is extended to the case of discontinuous coefficients across an arbitrary interface. Boundary and interface are implicitly described by level-set functions. The resulting linear system is not symmetric, and a proper multigrid solver is proposed. Numerical results show that second-order accuracy is achieved in both the solution and its gradient. Unlike other existing methods in the literature and mentioned above, variable high-jump coefficients do not affect (i) the monotonic decreasing of the error, which decays with second order accuracy in both the solutions and its gradient, or (ii) the multigrid efficiency, where the convergence factor does not depend on the coefficient ratio.

The plan of the paper is the following: in the next section we describe the model problem and introduce the level-set function and some notation. The third section is devoted to the description of the discretization of the model problem, with particular attention to the discretization of the boundary and interface conditions. Section 4 describes the multigrid approach with all the multigrid ingredients, consisting mainly of the relaxation scheme and the transfer (restriction and interpolation) operators. The last Section is devoted to numerical tests showing the second-order accuracy of the method and the optimal convergence factor of the multigrid approach.

## 2 Model Problem

In the whole paper we refer to the 2D case, although the method can be easily extended to higher dimensions. Let  $D = (-1, 1)^2$  be the computational domain and  $\Omega \subset D$  be a domain such that  $\partial\Omega \cap \partial D = \emptyset$ . Let us consider a partition  $\Omega = \{\Omega^+, \Omega^-\}$ , i.e.  $\Omega^+$  and  $\Omega^-$  are two non-empty domains such that  $\Omega^+ \cap \Omega^- = \emptyset$  and  $\Omega = \overline{\Omega^+} \cup \overline{\Omega^-}$ , where  $\overline{\Omega^\pm}$  denotes the closure of  $\Omega^\pm$ . We restrict our study to the case  $\partial\Omega^- \cap \partial\Omega = \emptyset$  (see Fig. 1). Let  $\Gamma$  be the *interface* separating the two subdomains, i.e.  $\Gamma = \partial\Omega^- \cap \partial\Omega^+$ , while the *boundary* of  $\Omega$  is  $\partial\Omega$ . We assume that both  $\partial\Omega$  and  $\Gamma$  are smooth curves. Consider the following problem:

$$\left\{ \begin{array}{l} -\nabla \cdot (\beta^\pm \nabla u^\pm) = f^\pm \text{ in } \Omega^\pm \\ \llbracket u \rrbracket = g_D \text{ on } \Gamma \\ \left[ \left[ \beta \frac{\partial u}{\partial n} \right] \right] = g_N \text{ on } \Gamma \\ u = g \text{ on } \partial\Omega \end{array} \right. \quad (1)$$

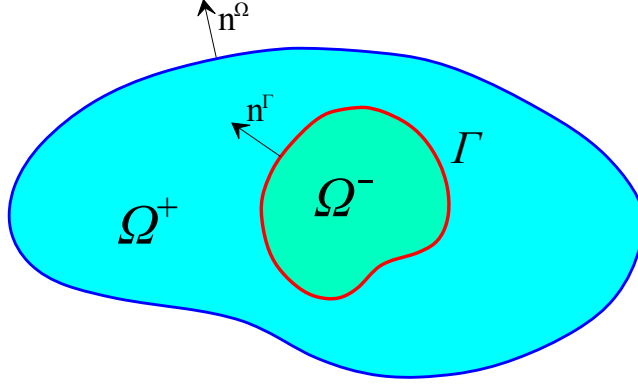


Fig. 1: Domain partition  $\Omega = \Omega^- \cup \Omega^+$  and the interface  $\Gamma$  separating the two subdomains along which we impose the jump conditions.

where  $\beta^-$  and  $\beta^+$  are positive smooth functions bounded away from zero. With  $[[\cdot]]$  we denote the jump across the interface  $\Gamma$ , i.e.

$$[[\omega]](\bar{x}, \bar{y}) = \lim_{\Omega^+ \ni (x,y) \rightarrow (\bar{x}, \bar{y})} \omega^+(x, y) - \lim_{\Omega^- \ni (x,y) \rightarrow (\bar{x}, \bar{y})} \omega^-(x, y).$$

for any  $(\bar{x}, \bar{y}) \in \Gamma$ .

**Remark 1** *Although we assign Dirichlet boundary conditions on  $\partial\Omega$ , the numerical method proposed in this paper can be easily extended to the more general case of Neumann or Robin boundary conditions, as proposed in [15]. Since the main focus of this paper is on interface conditions on  $\Gamma$ , we prescribe only Dirichlet boundary conditions on  $\partial\Omega$ .*

## 2.1 Level-set functions

The domains and the interface are implicitly known by two level set functions  $\phi$  and  $\phi^\Gamma$  in such a way:

$$\begin{aligned} \Omega &= \{(x, y) : \phi(x, y) < 0\}, \\ \Omega^- &= \{(x, y) : \phi^\Gamma(x, y) < 0 \text{ and } \phi(x, y) < 0\}, \\ \Omega^+ &= \{(x, y) : \phi^\Gamma(x, y) > 0 \text{ and } \phi(x, y) < 0\}, \\ \Gamma &= \{(x, y) : \phi^\Gamma(x, y) = 0 \text{ and } \phi(x, y) < 0\}. \end{aligned} \tag{2}$$

Level set methods for tracking interfaces are introduced and largely discussed, for example, in [49, 56]. For a fixed geometry, the level-set functions are not uniquely defined. A particular case of level-set function is the signed distance function:

$$\phi(x, y) = \begin{cases} -d((x, y), \partial\Omega) & \text{if } (x, y) \in \Omega, \\ d((x, y), \partial\Omega) & \text{if } (x, y) \notin \Omega, \end{cases}$$

where  $d((x, y), \partial\Omega) = \inf_{(\bar{x}, \bar{y}) \in \partial\Omega} d_e((x, y), (\bar{x}, \bar{y}))$  is the distance between a point and the set  $\partial\Omega$  ( $d_e$  is the Euclidean distance between points). The signed distance function  $\phi$  can be obtained, for example, by the reinitialization approach [57, 53, 20], namely as the steady-state solution of the following problem

$$\frac{\partial\phi}{\partial t} = \text{sign}(\phi_0) (1 - |\nabla\phi|), \quad \phi = \phi_0 \text{ at } t = 0, \tag{3}$$



where  $\phi_0$  is a generic level-set function representing  $\Omega$ , and  $t$  a fictitious time that represents an iterative parameter. A signed distance function is usually numerically more stable than a generic level-set function, since the latter may develop too steep (or too shallow) gradients. From now on we assume that  $\phi$  is the signed-distance function, possibly computed by Eq. (3). We observe that it is sufficient to solve Eq. (3) only for a few time steps, since we need to know the distance function only in a narrow band surrounding the interface/boundary.

The same argument can be repeated for the level-set function  $\phi^\Gamma$ , referred to the interface  $\Gamma$ .

The normal unit vectors to  $\partial\Omega$  and  $\Gamma$  are, respectively:

$$\mathbf{n} = \frac{\nabla\phi}{|\nabla\phi|}, \quad \mathbf{n}^\Gamma = \frac{\nabla\phi^\Gamma}{|\nabla\phi^\Gamma|},$$

where  $\phi$  and  $\phi^\Gamma$  are generic level-set functions (not necessarily signed distance functions).

## 2.2 Notation

Let  $N \geq 1$  be an integer and  $h = 2/N$  the spatial step. Let  $D_h = \{\mathbf{j}h, \mathbf{j} = (i, j) \in \{-N, -N+1, \dots, N-1, N\}^2\}$  be the discrete versions of  $D$ .  $D_h$  is the set of the *grid points*. Let  $\Omega_h^+ = \Omega^+ \cap D_h$  and  $\Omega_h^- = \Omega^- \cap D_h$  be the discrete versions of  $\Omega^+$  and  $\Omega^-$  respectively. Let  $\partial\Omega_h^+$  be the set of the *ghost points for  $\Omega^+$* , namely the grid points outside  $\Omega^+$  and such that one of the four neighbour grid points is inside  $\Omega^+$ , i.e.:

$$(x, y) \in \partial\Omega_h^+ \iff (x, y) \in D_h \setminus \Omega_h^+ \text{ and } \{(x \pm h, y), (x, y \pm h)\} \cap \Omega_h^+ \neq \emptyset.$$

Similarly, we define  $\partial\Omega_h^-$  the set of the *ghost points for  $\Omega^-$* , and  $\partial\Omega_h$  the set of the *ghost points for  $\Omega$* . Let us define  $\Gamma_h^- = \partial\Omega_h^- \setminus \partial\Omega_h$  and  $\Gamma_h^+ = \partial\Omega_h^+ \setminus \partial\Omega_h$ . We call  $N_i^+ = |\Omega_h^+|$ ,  $N_g^+ = |\Gamma_h^+|$ ,  $N_i^- = |\Omega_h^-|$ ,  $N_g^- = |\Gamma_h^-|$ ,  $N_g = |\partial\Omega_h|$ . Refer to Fig. 2 for clarity. Since  $\partial\Omega^- \cap \partial\Omega = \emptyset$  (see Fig. 1), we have  $\Gamma_h^- = \partial\Omega_h^-$ . We will use the following notation for discrete functions:  $w_{i,j} \approx w(ih, jh)$ ,  $w_P \approx w(P)$ .

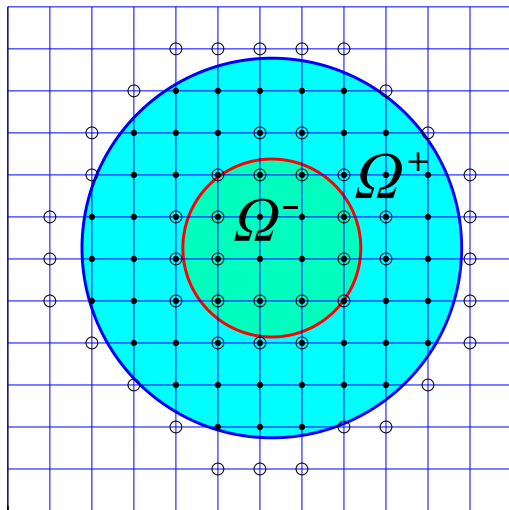


Fig. 2: Inside grid points and ghost points introduced in Sec. 2.2. In particular, the dot grid points inside  $\Omega^-$  represent the grid points of  $\Omega_h^-$ , the dot grid points inside  $\Omega^+$  and outside  $\Omega^-$  represent the grid points of  $\Omega_h^+$ , the unfilled circle grid points inside  $\Omega^-$  represent the grid points of  $\Gamma_h^+$ , the unfilled circle grid points inside  $\Omega^+$  and outside  $\Omega^-$  represent the grid points of  $\Gamma_h^-$ , the unfilled circle grid points outside  $\Omega^-$  and  $\Omega^+$  represent the grid points of  $\partial\Omega_h$ .

### 3 Discretization of the problem

The final linear system coming from the discretization of the problem will consist of a  $(N_i^+ + N_g^+ + N_i^- + N_g^- + N_g) \times (N_i^+ + N_g^+ + N_i^- + N_g^- + N_g)$  linear system. The  $N_i^-$  equations coming from the grid points of  $\Omega_h^-$  are obtained discretizing the first Eq. of (1) by usual central differences:

$$\beta_{i+1/2,j}^- (u_{i,j}^- - u_{i+1,j}^-) + \beta_{i-1/2,j}^- (u_{i,j}^- - u_{i-1,j}^-) + \beta_{i,j+1/2}^- (u_{i,j}^- - u_{i,j+1}^-) + \beta_{i,j-1/2}^- (u_{i,j}^- - u_{i,j-1}^-) = f_{i,j}^- h^2 \quad (4)$$

where  $\beta_{i\pm 1/2,j}^- = (\beta_{i,j}^- + \beta_{i\pm 1,j}^-)/2$ ,  $\beta_{i,j\pm 1/2}^- = (\beta_{i,j}^- + \beta_{i,j\pm 1}^-)/2$ . Similarly, we write an equation for each grid point of  $\Omega_h^+$ :

$$\beta_{i+1/2,j}^+ (u_{i,j}^+ - u_{i+1,j}^+) + \beta_{i-1/2,j}^+ (u_{i,j}^+ - u_{i-1,j}^+) + \beta_{i,j+1/2}^+ (u_{i,j}^+ - u_{i,j+1}^+) + \beta_{i,j-1/2}^+ (u_{i,j}^+ - u_{i,j-1}^+) = f_{i,j}^+ h^2 \quad (5)$$

Therefore, to close the linear system, we must write an equation for each ghost point  $G \in \Gamma_h^+ \cup \Gamma_h^- \cup \partial\Omega_h$ .

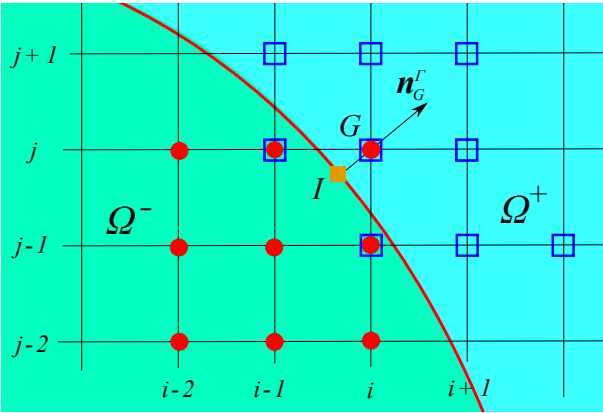


Fig. 3: In this figure  $G \in \Gamma_h^-$ . The nine-point stencil contained in  $\Omega_h^+ \cup \Gamma_h^+$  that serves to interpolate  $\tilde{u}^+$  is represented by unfilled squares (modified with respect to the standard central stencil); the nine-point stencil contained in  $\Omega_h^- \cup \Gamma_h^-$  that serves to interpolate  $\tilde{u}^-$  is represented by filled circles. Interface point  $I$  is represented by a filled square.

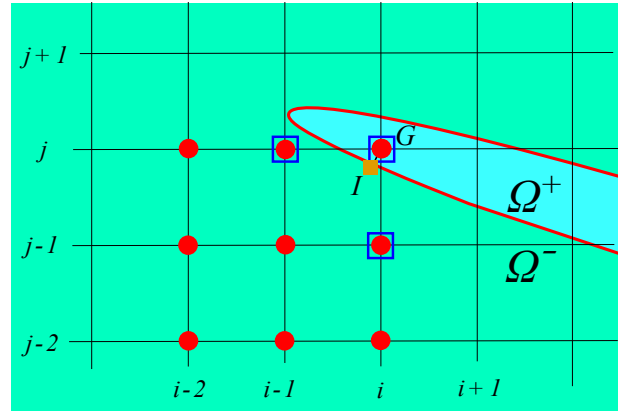


Fig. 4: In this figure  $G \in \Gamma_h^+$ . The nine-point stencil contained in  $\Omega_h^+ \cup \Gamma_h^+$  serving to interpolate  $\tilde{u}^+$  has been reduced to the three-point stencil represented by unfilled squares.

#### 3.1 Discretization of the interface conditions

Let  $G \in \Gamma_h^- \cup \Gamma_h^+$ . In order to find an extrapolated value for  $G$ , we discretize the interface conditions (second and third equations of (1)). Let us explain such discretization in detail.

First, we compute an approximation of the unit normal vector to  $\Gamma$  in  $G$  pointing from  $\Omega^-$  to  $\Omega^+$ , that is  $\mathbf{n}_G^\Gamma = (n_{G,x}^\Gamma, n_{G,y}^\Gamma) = (\nabla\phi^\Gamma / |\nabla\phi^\Gamma|)|_G$ , using a central finite-difference approximation for  $\nabla\phi^\Gamma$ . Since  $\phi^\Gamma$  is the signed distance function, the closest interface point to  $G$ , that we call  $I$ , is approximated by:

$$I = G - \mathbf{n}_G^\Gamma \cdot \phi^\Gamma(G). \quad (6)$$

Then, the equation of the linear system for the ghost point  $G$  is obtained discretizing one of the jump conditions (second and third equation of (1)): more precisely, if  $G \in \Gamma_h^-$  we use one of the two jump conditions, while if

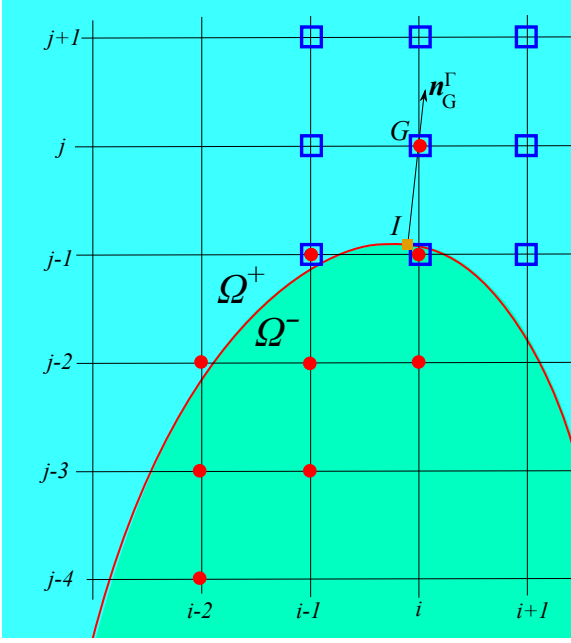


Fig. 5: In this figure  $G \in \Gamma_h^-$ . The nine-point stencil contained in  $\Omega_h^+ \cup \Gamma_h^+$  that serves to interpolate  $\tilde{u}^+$  is represented by unfilled squares; the nine-point stencil contained in  $\Omega_h^- \cup \Gamma_h^-$  that serves to interpolate  $\tilde{u}^-$  is modified with respect to the standard upwind stencil and is represented by filled circles.

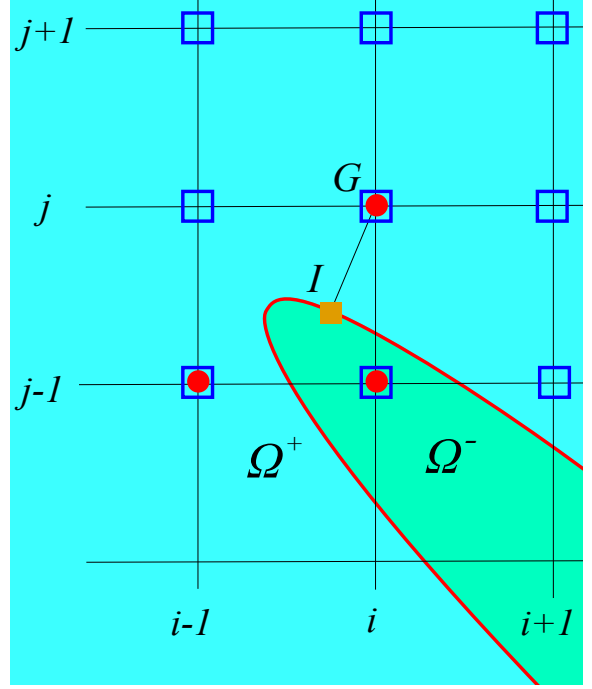


Fig. 6: In this figure  $G \in \Gamma_h^-$ . The nine-point stencil contained in  $\Omega_h^- \cup \Gamma_h^-$  serving to interpolate  $\tilde{u}^-$  has been reduced to the three-point stencil (filled circles).

$G \in \Gamma_h^+$  we use the other jump condition. Which jump condition has to be used in each case constitutes a choice, that can be based, for example, on the condition number of the resulting linear system. In fact, it is preferred to use the jump in the flux (third equation in (1)) if  $G$  is the ghost point for the domain where the coefficient  $\beta$  is greater, in order to obtain a better conditioned linear system. To explain this fact, let us suppose we want to discretize the equation for the ghost point  $G \in \Gamma^-$  and that  $\beta^- < \beta^+$ . If we discretize the jump in the flux (third equation of (1)) to construct the equation of the linear system, then the diagonal entry is multiplied by  $\beta^-$ , while some of the off-diagonal entries are multiplied by  $\beta^+ > \beta^-$ . The presence of larger off-diagonal values may lead to an ill-conditioned system.

Therefore:

- if  $\{G \in \Gamma_h^+ \text{ and } \beta^+(I) < \beta^-(I)\}$  or  $\{G \in \Gamma_h^- \text{ and } \beta^+(I) > \beta^-(I)\}$ , then the equation for the ghost point  $G$  is obtained from  $\llbracket u \rrbracket(I) = g_D(I)$ :

$$\boxed{\tilde{u}_h^+(I) - \tilde{u}_h^-(I) = g_D(I)} \quad (7)$$

- otherwise, it is obtained from  $\left[ \left[ \beta \frac{\partial u}{\partial n} \right] \right](I) = g_N(I)$ :

$$\boxed{(\beta^+ \nabla \tilde{u}_h^+ - \beta^- \nabla \tilde{u}_h^-)|_I \cdot \left( \frac{\nabla \tilde{\phi}_h^\Gamma}{|\nabla \tilde{\phi}_h^\Gamma|} \right)|_I = g_N(I)} \quad (8)$$

where  $\tilde{u}_h^+$  (resp.  $\tilde{u}_h^-$ ) is the biquadratic interpolant of  $u_h^+$  (resp.  $u_h^-$ ) in a suitable nine-point stencil contained in  $\Omega_h^+ \cup \Gamma_h^+$  (resp.  $\Omega_h^- \cup \Gamma_h^-$ ), and  $\tilde{\phi}_h^\Gamma$  is the biquadratic interpolant of  $\phi^\Gamma$  in a nine-point stencil surrounding  $I$ . What is left is the choice of the nine-point stencils contained in  $\Omega_h^- \cup \Gamma_h^-$  and  $\Omega_h^+ \cup \Gamma_h^+$ .

Let us recall that the biquadratic interpolant of a function  $\omega(x, y)$  is a polynomial:

$$\tilde{\omega}(x, y) = a_1 x^2 y^2 + a_2 x^2 y + a_3 x y^2 + a_4 x^2 + a_5 y^2 + a_6 x y + a_7 x + a_8 y + a_9$$

whose coefficients  $a_i$  are obtained imposing  $\tilde{\omega}(\bar{x}, \bar{y}) = \omega(\bar{x}, \bar{y})$ , for each  $(\bar{x}, \bar{y})$  belonging to the nine-point stencil.

### 3.1.1 Choice of the stencil

Let us suppose that  $G \in \Gamma_h^-$  (if  $G \in \Gamma_h^+$  the procedure is the same, provided that subscripts  $+$  and  $-$  are interchanged).

**3.1.1.1 Stencil contained in  $\Omega_h^- \cup \Gamma_h^-$ .** The nine-point stencil contained in  $\Omega_h^- \cup \Gamma_h^-$  is chosen in upwind direction, using the same technique described in [15, 13], i.e.:

$$St_9^U = \{G + h(s_x k_1, s_y k_2) : (k_1, k_2) \in \{0, 1, 2\}^2\}, \quad (9)$$

where  $s_x = \text{sign}(x_I - x_G)$  and  $s_y = \text{sign}(y_I - y_G)$ , with  $G \equiv (x_G, y_G)$  and  $I \equiv (x_I, y_I)$ . We call the nine-point stencil (9) *standard upwind stencil* and it is contained in  $\Omega_h^- \cup \Gamma_h^-$  provided that the grid is sufficiently fine (i.e. the spatial step  $h$  is sufficiently small) with respect to the curvature of the interface (such as in Fig. 3). For coarser grids (that must be considered in the multigrid approach, see Sec. 4), it may happen that the stencil is not entirely contained in  $\Omega_h^- \cup \Gamma_h^-$  (see Fig. 5). In this case, a *modified* nine-point stencil is chosen when available (Fig. 5), or in the worst case the stencil is reduced to a first-order accurate three-point stencil (Fig. 6), as explained later. Since this latter reduction occurs quite rarely in a fine grid, the overall second-order accuracy is not affected (as shown in numerical tests).

Assuming  $n_{G,x}^\Gamma > 0$  and  $n_{G,y}^\Gamma > 0$  (the other cases are treated similarly), the (modified) nine-point stencil is chosen using the following algorithm. If  $|x_I - x_G| < |y_I - y_G|$  (as in Fig. 5), the nine-point stencil will be composed by three points of each of the columns  $i$ ,  $i - 1$  and  $i - 2$ ; while if  $|x_I - x_G| \geq |y_I - y_G|$  it will be composed by three points of each of the rows  $j$ ,  $j - 1$  and  $j - 2$ . Let us suppose  $|x_I - x_G| < |y_I - y_G|$  (the opposite case is treated similarly).

- The three points of the column  $i$  are:

$$(i, j)h, (i, j - 1)h, (i, j - 2)h.$$

These three points belong to  $\Omega_h^- \cup \Gamma_h^-$ , since  $(i, j - 1)h \equiv G \in \Omega_h^-$ .

- The three points of the column  $i - 1$  are

$$(i - 1, j)h, (i - 1, j - 1)h, (i - 1, j - 2)h$$

if they belong to  $\Omega_h^- \cup \Gamma_h^-$ , otherwise we choose:

$$(i - 1, j - 1)h, (i - 1, j - 2)h, (i - 1, j - 3)h \quad (10)$$

if they belong to  $\Omega_h^- \cup \Gamma_h^-$ , otherwise we reduce the stencil as described later.

- The three points of the column  $i - 2$  are

$$(i - 2, j)h, (i - 2, j - 1)h, (i - 2, j - 2)h$$

if they belong to  $\Omega_h^- \cup \Gamma_h^-$ , otherwise we choose:

$$(i - 2, j - 1)h, (i - 2, j - 2)h, (i - 2, j - 3)h$$

if they belong to  $\Omega_h^- \cup \Gamma_h^-$ , otherwise, if the three points for the column  $i - 1$  were those indicated in Eq. (10), we choose:

$$(i - 2, j - 2)h, (i - 2, j - 3)h, (i - 2, j - 4)h$$

if they belong to  $\Omega_h^- \cup \Gamma_h^-$  (this is the case illustrated in Fig. 5), otherwise we reduce the stencil as described later.

**Reduction of the stencil contained in  $\Omega_h^- \cup \Gamma_h^-$ .** If it is not possible to build the nine-point stencil, we revert to a more robust (less accurate) three-point stencil (Fig. 6):

$$(i, j)h, (i - 1, j)h, (i, j - 1)h.$$

In this case a linear interpolation is used instead of a biquadratic interpolation. Note that these three points belong to  $\Omega_h^- \cup \Gamma_h^-$ , since  $G \equiv (i, j - 1)h \in \Omega_h^-$ .

**3.1.1.2 Stencil contained in  $\Omega_h^+ \cup \Gamma_h^+$ .** The nine-point stencil contained in  $\Omega_h^+ \cup \Gamma_h^+$  is:

$$St_9^C = \{G + h(k_1, k_2) : (k_1, k_2) \in \{-1, 0, 1\}^2\}, \quad (11)$$

We call the nine-point stencil (11) *standard central stencil* (see Figs. 5 and 6). If it is not contained in  $\Omega_h^+ \cup \Gamma_h^+$ , a *modified* nine-point stencil is chosen (Fig. 3) or, in the worst case, the stencil is reduced to a three-point stencil (Fig. 4).

The (modified) nine-point stencil contained in  $\Omega_h^+ \cup \Gamma_h^+$  will be set as follows: if  $|x_G - x_I| \geq |y_G - y_I|$  (as in Fig. 3) it will be composed by three points of each of the rows  $j - 1$ ,  $j$  and  $j + 1$ ; while if  $|x_G - x_I| < |y_G - y_I|$  it will be composed by three points of each of the columns  $i - 1$ ,  $i$  and  $i + 1$ . Let us suppose  $|x_G - x_I| \geq |y_G - y_I|$  (the opposite case is treated similarly). Then:

- The three points of the row  $j$  are:

$$(i - 1, j)h, (i, j)h, (i + 1, j)h.$$

Since  $(i, j)h \equiv G \in \Omega_h^+$ , such three points belong to  $\Omega_h^+ \cup \Gamma_h^+$ .

- The three points of the row  $j + 1$  are

$$(i - 1, j + 1)h, (i, j + 1)h, (i + 1, j + 1)h$$

if all of them belong to  $\Omega_h^+ \cup \Gamma_h^+$ , otherwise we choose one of the following two triples:

$$\{(i - 2, j + 1)h, (i - 1, j + 1)h, (i, j + 1)h\} \text{ or}$$

$$\{(i, j + 1)h, (i + 1, j + 1)h, (i + 2, j + 1)h\}$$

if one of them is contained in  $\Omega_h^+ \cup \Gamma_h^+$ , otherwise we reduce the stencil as described later.

- The three points of the row  $j - 1$  are

$$(i - 1, j - 1)h, (i, j - 1)h, (i + 1, j - 1)h$$

if all of them belong to  $\Omega_h^+ \cup \Gamma_h^+$ , otherwise we choose one of the following two triples:

$$\{(i - 2, j - 1)h, (i - 1, j - 1)h, (i, j - 1)h\} \text{ or}$$

$$\{(i, j - 1)h, (i + 1, j - 1)h, (i + 2, j - 1)h\}$$

if one of them is contained in  $\Omega_h^+ \cup \Gamma_h^+$ , otherwise we reduce the stencil as described later.

**Reduction of the stencil contained in  $\Omega_h^+ \cup \Gamma_h^+$ .** If it is not possible to build the nine-point stencil, we revert to a more robust (less accurate) three-point stencil (Fig. 4):

$$(i, j)h, (i - 1, j)h, (i, j - 1)h.$$

Note that these three points belong to  $\Omega_h^+ \cup \Gamma_h^+$ , since  $G \equiv (i, j)h \in \Omega_h^+$ .

### 3.2 Discretization of the boundary conditions

Let  $G \in \partial\Omega_h$ . In order to find an extrapolated value for  $G$ , we discretize the boundary condition on  $\Omega$ , i.e. the fourth equation of (1). First, we approximate the outward unit normal in  $G$  by the formula  $\mathbf{n}_G = (n_G^x, n_G^y) = \nabla\phi / |\nabla\phi|$ , where  $\nabla\phi$  is discretized by central difference in  $G$ . Then, the closest boundary point to  $G$ , that we call  $B$ , is computed similarly to (6):

$$B = G - \phi(G)\mathbf{n}_G. \quad (12)$$

Finally, the equation of the linear system related to the ghost point  $G$  is:

$$\tilde{u}(B) = g(B) \quad (13)$$

where  $\tilde{u}$  is the biquadratic interpolant of  $u$  on the upwind nine-point stencil  $St_9^U$ :

$$St_9^U = \{G + h(s_x k_1, s_y k_2) : (k_1, k_2) \in \{0, 1, 2\}^2\}, \quad (14)$$

where  $s_x = \text{sign}(x_B - x_G)$  and  $s_y = \text{sign}(y_B - y_G)$ , with  $G \equiv (x_G, y_G)$  and  $B \equiv (x_B, y_B)$ . This stencil may not be contained entirely in  $\Omega_h^+ \cup \Gamma_h^+$ . In such cases it is modified in the same way as in Sec. 3.1.1.1.

## 4 Multigrid approach

The discretization presented in Sec. 3 leads to a sparse non-symmetric linear system that will be solved efficiently by a multigrid approach. We refer the reader to [59] for a comprehensive presentation of multigrid methods. In this paper we confine the description on how the ingredients of standard multigrid (relaxation scheme, transfer operators) are modified for this specific problem. The first step consists of providing a proper relaxation scheme. Gauss-Seidel and (weighted) Jacobi schemes do not converge for this specific problems unless a special treatment is performed for the relaxation scheme on the ghost points, as described in the following section.

### 4.1 Relaxation scheme

The relaxation scheme aims at maintaining a Jacobi- or Gauss-Seidel-like iteration scheme for internal points, and propose a proper relaxation scheme for ghost points. For the clarity of description, we describe the scheme for the Jacobi-like scheme (for internal points), although easy generalization can be obtained for weighted-Jacobi or Gauss-Seidel schemes (which are the schemes that we use in practice, since they are more suitable for multigrid techniques due to the smoothing property, see [59, Ch. 2.1]). The whole scheme is obtained discretizing the following *associate time-dependent problem* in space and (fictitious) time:

$$\begin{aligned} \frac{\partial u^\pm}{\partial t} &= \mu^\pm (f^\pm + \nabla \cdot (\beta^\pm \nabla u^\pm)) \quad \text{in } \Omega^\pm \\ \frac{\partial u^{s_1}}{\partial t} &= \mu_D (g_D - [u]) \quad \text{on } \Gamma \\ \frac{\partial u^{s_2}}{\partial t} &= \mu_N \left( g_N - \left[ \beta \frac{\partial u}{\partial n} \right] \right) \quad \text{on } \Gamma \\ \frac{\partial u}{\partial t} &= \mu_B (g - u) \quad \text{on } \partial\Omega \end{aligned} \quad (15)$$

where  $s_1, s_2 \in \{-, +\}$  and  $s_1 \neq s_2$ . The choice of  $s_1$  and  $s_2$  depends on the value of  $\beta$  in order to have a better preconditioner for the linear system, as explained in Sec. 3.2. In detail:

$$\begin{aligned} s_1 = +, \quad s_2 = - & \quad \text{if } \beta^+ \leq \beta^-, \\ s_1 = -, \quad s_2 = + & \quad \text{if } \beta^+ > \beta^-. \end{aligned}$$

Let us describe this relaxation scheme in detail. For a grid point  $(i, j)h \in \Omega_h^-$ , the iterative scheme is obtained discretizing the first equation of (15) by forward Euler in time and by (4) in space:

$$\begin{aligned} u_{i,j}^{-(n+1)} = u_{i,j}^{-(n)} + \mu_{i,j}^- \Delta t f_{i,j}^- + \frac{\mu_{i,j}^- \Delta t}{h^2} & \left( \beta_{i+1/2,j}^- \left( u_{i,j}^{-(n)} - u_{i+1,j}^{-(n)} \right) + \beta_{i-1/2,j}^- \left( u_{i,j}^{-(n)} - u_{i-1,j}^{-(n)} \right) \right. \\ & \left. + \beta_{i,j+1/2}^- \left( u_{i,j}^{-(n)} - u_{i,j+1}^{-(n)} \right) + \beta_{i,j-1/2}^- \left( u_{i,j}^{-(n)} - u_{i,j-1}^{-(n)} \right) \right) \end{aligned} \quad (16)$$

where  $\mu_{i,j}^-$  is chosen in such a way (16) becomes a Jacobi-like scheme, i.e.:

$$\mu_{i,j}^- \Delta t = \frac{h^2}{\beta_{i-1/2,j}^- + \beta_{i+1/2,j}^- + \beta_{i,j-1/2}^- + \beta_{i,j+1/2}^-}. \quad (17)$$

If  $(i, j)h \in \Omega_h^+$  the iteration scheme is similar and is obtained by replacing the subscript  $-$  with  $+$ :

$$\begin{aligned} u_{i,j}^{+(n+1)} = u_{i,j}^{+(n)} + \mu_{i,j}^+ \Delta t f_{i,j}^+ + \frac{\mu_{i,j}^+ \Delta t}{h^2} & \left( \beta_{i+1/2,j}^+ \left( u_{i,j}^{+(n)} - u_{i+1,j}^{+(n)} \right) + \beta_{i-1/2,j}^+ \left( u_{i,j}^{+(n)} - u_{i-1,j}^{+(n)} \right) \right. \\ & \left. + \beta_{i,j+1/2}^+ \left( u_{i,j}^{+(n)} - u_{i,j+1}^{+(n)} \right) + \beta_{i,j-1/2}^+ \left( u_{i,j}^{+(n)} - u_{i,j-1}^{+(n)} \right) \right) \end{aligned} \quad (18)$$

We observe that in practice we do not need to define both values  $\mu_{i,j}^-$  and  $\Delta t$  for Eqs. (16), (18), but only the product  $\mu_{i,j}^\pm \Delta t = \mu_{i,j}^\pm \Delta t$  according to Eq. (17).

Now, let us consider a ghost point  $G \in \partial\Omega_h$ . The iterative scheme for  $G$  is obtained discretizing the fourth equation of (15) by forward Euler in time and by (13) in space:

$$u_G^{(n+1)} = u_G^{(n)} + \mu_B \Delta t \left( g(B) - \tilde{u}^{(n)}(B) \right), \quad (19)$$

where  $B$  is the projection point on the boundary  $\partial\Omega$  obtained by (12).

If  $G \in \Gamma_h^-$ , the iterative scheme for  $G$  is obtained discretizing the second or third equation of (15), more precisely, the second equation if  $s_1 = -$ , the third equation if  $s_2 = -$ . This choice is in accord with the discretization of the interface conditions described in Sec. 3.2. Recalling the choice (7) or (8), and the (6), we summarize the iteration as follows:

- if  $\beta^+(I) > \beta^-(I)$ , then the iteration for the ghost point  $G \in \Gamma_h^-$  is:

$$u_G^{-(n+1)} = u_G^{-(n)} + \mu_D \Delta t \left( g_D(I) - \left( \tilde{u}_h^{+(n)}(I) - \tilde{u}_h^{-(n)}(I) \right) \right) \quad (20)$$

- otherwise, it is:

$$u_G^{-(n+1)} = u_G^{-(n)} + \mu_N \Delta t \left( g_N(I) - \left( \beta^+ \nabla \tilde{u}_h^{+(n)} - \beta^- \nabla \tilde{u}_h^{-(n)} \right) \Big|_I \cdot \left( \frac{\nabla \tilde{\phi}_h^\Gamma}{|\nabla \tilde{\phi}_h^\Gamma|} \right) \Big|_I \right) \quad (21)$$

On the contrary, the iterative equation for a ghost point  $G \in \Gamma_h^+$  will be set as follows.

- if  $\beta^+(I) > \beta^-(I)$ , then the equation for the ghost point  $G \in \Gamma_h^+$  is:

$$u_G^{+(n+1)} = u_G^{+(n)} + \mu_N \Delta t \left( g_N(I) - \left( \beta^+ \nabla \tilde{u}_h^{+(n)} - \beta^- \nabla \tilde{u}_h^{-(n)} \right) \Big|_I \cdot \left( \frac{\nabla \tilde{\phi}_h^\Gamma}{|\nabla \tilde{\phi}_h^\Gamma|} \right) \Big|_I \right) \quad (22)$$

- otherwise, it is:

$$u_G^{+(n+1)} = u_G^{+(n)} + \mu_D \Delta t \left( g_D(I) - \left( \tilde{u}_h^{+(n)}(I) - \tilde{u}_h^{-(n)}(I) \right) \right) \quad (23)$$

Up to now, nothing has been said about the sign of the constants  $\mu_D$ ,  $\mu_N$  and  $\mu_B$ . This is a crucial point in order to make the whole iterative process convergent. What we request for stability is, in fact, that the derivative of the right-hand side of (20)-(23) with respect to  $u_G^{\pm(n)}$  is positive and less than one. For example, considering the iteration (20), the derivative of the right-hand side, that we call  $c_G^-$ , is:

$$c_G^- = 1 + \mu_D \Delta t \frac{\partial \tilde{u}_h^-(I)}{\partial u_G^{-(n)}}.$$

The stability is attained for  $0 < c_G^- \leq 1$ . It can be proved that see (Eq. (55) in Appendix 1)

$$\frac{\partial \tilde{u}_h^-(I)}{\partial u_G^{-(n)}} \geq 0. \quad (24)$$

Therefore, the condition  $c_G^- \leq 1$  is ensured by  $\mu_D < 0$ , while the condition  $0 < c_G^-$  implies

$$|\mu_D| \Delta t < \left( \frac{\partial \tilde{u}_h^-(I)}{\partial u_G^{-(n)}} \right)^{-1}.$$

This condition must hold for every possible value of  $\frac{\partial \tilde{u}_h^-(I)}{\partial u_G^{-(n)}}$ , which in fact depends on the vector  $G - I$ . It can be shown that (see Eq. (56) in Appendix 1):

$$\sup_{|G-I| \leq h} \left( \frac{\partial \tilde{u}_h^-(I)}{\partial u_G^{-(n)}} \right) = 1 \quad (25)$$

and then the stability conditions for (20) finally read:

$$\mu_D < 0, \quad |\mu_D| \Delta t < 1. \quad (26)$$

Let us now consider the iteration (21). The derivative  $c_G^-$  of the right-hand side with respect to  $u_G^{-(n)}$  is:

$$c_G^- = 1 + \mu_N \Delta t \frac{\partial (\beta^- \nabla \tilde{u}_h^-(I) \cdot \tilde{\mathbf{n}}_I^\Gamma)}{\partial u_G^{-(n)}}.$$

where  $\tilde{\mathbf{n}}_I^\Gamma = \frac{\nabla \tilde{\phi}_h^\Gamma(I)}{|\nabla \tilde{\phi}_h^\Gamma(I)|}$ . The stability condition is  $0 < c_G^- \leq 1$ . Since  $\tilde{\mathbf{n}}_I^\Gamma$  points from  $\Omega^-$  to  $\Omega^+$  and the stencil is chosen in upwind direction, then it can be shown that (see Eq. (58) in Appendix 1)

$$\frac{\partial (\beta^- \nabla \tilde{u}_h^-(I) \cdot \tilde{\mathbf{n}}_I^\Gamma)}{\partial u_G^{-(n)}} \geq 0. \quad (27)$$



Therefore, the condition  $c_G^- \leq 1$  is satisfied when  $\mu_N < 0$ . Condition  $0 < c_G^-$  implies

$$|\mu_N| \Delta t < \left( \frac{\partial (\beta^- \nabla \tilde{u}_h^-(I) \cdot \tilde{\mathbf{n}}_I^\Gamma)}{\partial u_G^{-(n)}} \right)^{-1}.$$

As before, this condition must be satisfied for each possible value of  $\frac{\partial (\beta^- \nabla \tilde{u}_h^-(I) \cdot \tilde{\mathbf{n}}_I^\Gamma)}{\partial u_G^{-(n)}}$ , that depends on  $G - I$ . It can be shown that (see Eq. (59) in Appendix 1):

$$\sup_{|G-I| \leq h} \left( \frac{\partial (\beta^- \nabla \tilde{u}_h^-(I) \cdot \tilde{\mathbf{n}}_I^\Gamma)}{\partial u_G^{-(n)}} \right) \leq \frac{3\beta^-}{\sqrt{2}h}. \quad (28)$$

Finally, the stability conditions for (21) read:

$$\mu_N < 0, \quad \frac{|\mu_N| \Delta t}{h} < \frac{\sqrt{2}}{3\beta^-}. \quad (29)$$

By the same arguments, the stability conditions for the iteration (22) are:

$$\mu_N < 0, \quad \frac{|\mu_N| \Delta t}{h} < \frac{\sqrt{2}}{3\beta^+}, \quad (30)$$

while, for the iteration (23) are:

$$\mu_D > 0, \quad \mu_D \Delta t < 1. \quad (31)$$

Finally, observe that the conditions on  $\mu_B$  are (see (19)):

$$\mu_B > 0, \quad \mu_B \Delta t < 1. \quad (32)$$

#### 4.1.1 Changing of notation

For simplicity, we want to keep a suitable notation such that constants  $\mu_D$  and  $\mu_N$  are always positive. To this purpose, we change the associate time-dependent problem (15) as follows:

$$\begin{aligned} \frac{\partial u^\pm}{\partial t} &= \mu^\pm (f^\pm + \nabla \cdot (\beta^\pm \nabla u^\pm)) \text{ in } \Omega^\pm \\ \frac{\partial u^{s_1}}{\partial t} &= s_1 \mu_D (g_D - \llbracket u \rrbracket) \text{ on } \Gamma \\ \frac{\partial u^{s_2}}{\partial t} &= \mu_N \left( \left[ \left[ \beta \frac{\partial u}{\partial n} \right] \right] - g_N \right) \text{ on } \Gamma \\ \frac{\partial u}{\partial t} &= \mu_B (g - u) \text{ on } \partial\Omega. \end{aligned} \quad (33)$$

The iteration equations of the interface conditions (20)-(23) become:

- if  $\beta^+(I) > \beta^-(I)$ , then the equation for the ghost point  $G \in \Gamma_h^-$  is:

$$u_G^{-(n+1)} = u_G^{-(n)} - \mu_D \Delta t \left( g_D(I) - \left( \tilde{u}_h^{+(n)}(I) - \tilde{u}_h^{-(n)}(I) \right) \right) \quad (34)$$

- otherwise, it is:

$$u_G^{-(n+1)} = u_G^{-(n)} - \mu_N \Delta t \left( g_N(I) - \left( \beta^+ \nabla \tilde{u}_h^{+(n)} - \beta^- \nabla \tilde{u}_h^{-(n)} \right) \Big|_I \cdot \left( \frac{\nabla \tilde{\phi}_h}{|\nabla \tilde{\phi}_h|} \right) \Big|_I \right) \quad (35)$$

- if  $\beta^+(I) > \beta^-(I)$ , then the equation for the ghost point  $G \in \Gamma_h^+$  is:

$$u_G^{+(n+1)} = u_G^{+(n)} - \mu_N \Delta t \left( g_N(I) - \left( \beta^+ \nabla \tilde{u}_h^{+(n)} - \beta^- \nabla \tilde{u}_h^{-(n)} \right) \Big|_I \cdot \left( \frac{\nabla \tilde{\phi}_h}{|\nabla \tilde{\phi}_h|} \right) \Big|_I \right) \quad (36)$$

- otherwise, it is:

$$u_G^{+(n+1)} = u_G^{+(n)} + \mu_D \Delta t \left( g_D(I) - \left( \tilde{u}_h^{+(n)}(I) - \tilde{u}_h^{-(n)}(I) \right) \right) \quad (37)$$

#### 4.1.2 Choosing constants $\mu_B$ , $\mu_D$ and $\mu_N$

According to the new notation introduced in the previous section 4.1.1, the conditions (26), (29), (30) and (31) on the constants  $\mu_D$  and  $\mu_N$  become:

$$\mu_D \Delta t < 1, \quad \frac{\mu_N \Delta t}{h} < \frac{\sqrt{2}}{3\beta^\pm}. \quad (38)$$

The conditions on the positive constant  $\mu_B$  remain the (32).

We observe that in practice we do not need to define all four values  $\mu_D$ ,  $\mu_N$ ,  $\mu_B$  and  $\Delta t$  for Eqs. (19), (34), (35), (36), (37), but only the products  $\mu_B^{\Delta t} = \mu_B \Delta t$ ,  $\mu_D^{\Delta t} = \mu_D \Delta t$  and  $\mu_N^{\Delta t} = \mu_N \Delta t$ . In the numerical tests of Sec. 5 we use  $\mu_B^{\Delta t} = \mu_D^{\Delta t} = 0.9$  and  $\mu_N^{\Delta t} = 0.9 \frac{\sqrt{2} h}{3 \max\{\beta^+, \beta^-\}}$  (that satisfy the stability conditions (32), (38)).

#### 4.1.3 Smoothing property

As mentioned at the beginning of Sec. 4.1, it is known that the Jacobi scheme is not a proper smoother for the multigrid algorithm (see, for instance, [59, Ch. 2.1]). Therefore, we need to replace the Jacobi-like scheme introduced in Sec. 4.1 with a relaxation scheme that holds the smoothing property, such as the Gauss-Seidel scheme or the weighted Jacobi scheme (with weight  $\omega = 4/5$  in 2D). In the following, we revert as example to a Gauss-Seidel relaxation scheme. The smoothing property of the Gauss-Seidel scheme depends on the order chosen for the variables. It is well known (see [59, Ch. 2.1]) that the Gauss-Seidel Red-Black (GS-RB) scheme is a better smoother with respect to the Gauss-Seidel Lexicographic (GS-LEX) scheme. Anyway we study for simplicity the smoothing properties of the GS-LEX scheme and we compare the convergence factor with the one predicted by the Local Fourier Analysis for rectangular domains (see [59, Ch. 4.6.1] for more details), since the main goal of this paper is to show the efficiency of the method for complex geometries and not the choice of the best relaxation scheme. In order to obtain a more efficient multigrid method, a GS-RB can be easily employed instead of the GS-LEX (this is behind the scope of the paper).

Finally, we switch from the relaxation scheme described in Sec. 4.1 to a Gauss-Seidel version, namely we update the variable on which we are iterating and we use such updated value for the following iterations on the other variables. The only thing is left to choose is the order of the iterations. We use a lexicographic order for inner equations, and any order for interface and boundary conditions.

In detail, we order the grid points according to the following list:

$$\{\partial\Omega_h, \Gamma_h^-, \Gamma_h^+, \Omega_h^-, \Omega_h^+\}.$$

The order within any set of grid points of this list is arbitrary, except for grid points of  $\Omega_h^-$  and  $\Omega_h^+$ , where the lexicographic order is used, i.e.:

$$(x', y') \leq (x'', y'') \iff \begin{cases} x' < x'' \\ \text{or} \\ x' = x'' \text{ and } y' < y''. \end{cases}$$

In order to avoid that the boundary effects degrade the convergence factor, we perform some extra-relaxations on two suitable layers surrounding respectively the interface and the boundary. In detail, we choose a positive integer  $\lambda$  and a positive parameter  $\delta$ , and we introduce two additional sets of grid points:

$$\begin{aligned}\Omega_h^{(\delta)} &= \{P \in \Omega_h \text{ such that } d(P, \partial\Omega) < \delta\}, \\ \Omega_h^{\pm(\delta)} &= \{P \in \Omega_h^{\pm} \text{ such that } d(P, \Gamma) < \delta\}.\end{aligned}$$

One single relaxation includes some over-relaxations on  $\Omega_h^{(\delta)}$  and  $\Omega_h^{\pm(\delta)}$  and is represented by the Algorithm 1. Similarly to [15], we experienced that a good choice is:

$$\lambda = 5, \quad \delta = 5h. \quad (39)$$

## 4.2 Multigrid components

Let us extend the notation of Sec. 2.2. For a grid with spatial step  $h$ , we denote:

$$\Omega_h^{--} = \Omega_h^- \cup \Gamma_h^-, \quad \Omega_h^{++} = \Omega_h^+ \cup \Gamma_h^+.$$

Let us define the set of functions defined on a subset  $I_h$  of the grid:

$$S(I_h) = \{w_h : I_h \rightarrow \mathbb{R}\}, \text{ for any } I_h \subseteq D_h,$$

and then the set of functions defined on internal points:

$$\bar{S}(\Omega_h) = S(\Omega_h^- \cup \Gamma_h^-) \times S(\Omega_h^+ \cup \Gamma_h^+).$$

The discrete differential operators of the elliptic equation can be expressed by:

$L_h^- : S(\Omega_h^{--}) \times S(\Omega_h^{--}) \rightarrow S(\Omega_h^-)$  such that

$$\begin{aligned}L_h^-(\beta_h^-, u_h^-)_{i,j} &= \frac{1}{h^2} \left( \beta_{i+1/2,j}^- (u_{i,j}^- - u_{i+1,j}^-) + \beta_{i-1/2,j}^- (u_{i,j}^- - u_{i-1,j}^-) \right. \\ &\quad \left. + \beta_{i,j+1/2}^- (u_{i,j}^- - u_{i,j+1}^-) + \beta_{i,j-1/2}^- (u_{i,j}^- - u_{i,j-1}^-) \right) \text{ for any } (i,j)h \in \Omega^-, \end{aligned}$$

$L_h^+ : S(\Omega_h^{++}) \times S(\Omega_h^{++}) \rightarrow S(\Omega_h^+)$  such that

$$\begin{aligned}L_h^+(\beta_h^+, u_h^+)_{i,j} &= \frac{1}{h^2} \left( \beta_{i+1/2,j}^+ (u_{i,j}^+ - u_{i+1,j}^+) + \beta_{i-1/2,j}^+ (u_{i,j}^+ - u_{i-1,j}^+) \right. \\ &\quad \left. + \beta_{i,j+1/2}^+ (u_{i,j}^+ - u_{i,j+1}^+) + \beta_{i,j-1/2}^+ (u_{i,j}^+ - u_{i,j-1}^+) \right) \text{ for any } (i,j)h \in \Omega^+, \end{aligned}$$

and then they can be summarized as a unique operator  $L_h$ :

$L_h : \bar{S}(\Omega_h) \times \bar{S}(\Omega_h) \rightarrow S(\Omega_h)$  such that

$$L_h(\beta_h, u_h)(P) = \begin{cases} L_h^-(\beta_h^-, u_h^-) & \text{if } P \in \Omega_h^- \\ L_h^+(\beta_h^+, u_h^+) & \text{if } P \in \Omega_h^+ \end{cases}$$

where  $\beta_h = (\beta_h^-, \beta_h^+)$ ,  $u_h = (u_h^-, u_h^+)$ .

---

**Algorithm 1** One single relaxation includes some over-relaxations in the vicinity of the interface and boundary.

---

```

for  $i = 1 \rightarrow \lambda$  do

  for all  $G \in \partial\Omega_h$  do
    perform the iteration equation (19);
  end for
  for all  $G \in \Gamma_h^-$  do
    perform the iteration equation (34) or (35);
  end for
  for all  $G \in \Gamma_h^+$  do
    perform the iteration equation (36) or (37);
  end for
  for all  $P \in \Omega_h^{-(\delta)}$  do
    perform the iteration equation (16);
  end for
  for all  $P \in \Omega_h^{+(\delta)}$  do
    perform the iteration equation (18);
  end for
end for

```

```

for all  $G \in \partial\Omega_h$  do
  perform the iteration equation (19);
end for
for all  $G \in \Gamma_h^-$  do
  perform the iteration equation (34) or (35);
end for
for all  $G \in \Gamma_h^+$  do
  perform the iteration equation (36) or (37);
end for
for all  $P \in \Omega_h^-$  do
  perform the iteration equation (16);
end for
for all  $P \in \Omega_h^+$  do
  perform the iteration equation (18);
end for

```

---

The discrete jump operators become:

$[\cdot, \cdot]_h^- : \bar{S}(\Omega_h) \times \bar{S}(\Omega_h) \rightarrow S(\Gamma_h^-)$  such that

$$[\beta_h, u_h]_h^-(G) = \begin{cases} \tilde{u}_h^+(I) - \tilde{u}_h^-(I) \\ \text{or} \\ (\beta^+ \nabla \tilde{u}_h^+ - \beta^- \nabla \tilde{u}_h^-)|_I \cdot \left( \frac{\nabla \tilde{\phi}_h^\Gamma}{|\nabla \tilde{\phi}_h^\Gamma|} \right) \Big|_I \end{cases}$$

for any  $G \in \Gamma_h^-$ , according to the choice (7) or (8),

$[\cdot, \cdot]_h^+ : \bar{S}(\Omega_h) \times \bar{S}(\Omega_h) \rightarrow S(\Gamma_h^+)$  such that

$$[\beta_h, u_h]_h^+(G) = \begin{cases} \tilde{u}_h^+(I) - \tilde{u}_h^-(I) \\ \text{or} \\ (\beta^+ \nabla \tilde{u}_h^+ - \beta^- \nabla \tilde{u}_h^-)|_I \cdot \left( \frac{\nabla \tilde{\phi}_h^\Gamma}{|\nabla \tilde{\phi}_h^\Gamma|} \right) \Big|_I \end{cases}$$

for any  $G \in \Gamma_h^+$ , according to the choice (7) or (8).

Discrete right-hand sides of the jump conditions are summarized by a grid function  $g_h^+ \in S(\Gamma_h^+)$  [ $g_h^- \in S(\Gamma_h^-)$ ] such that  $g_h^+(G) = g_D(I)$  or  $g_N(I)$  [ $g_h^-(G) = g_D(I)$  or  $g_N(I)$ ], for any  $G \in \Gamma_h^+$  [ $G \in \Gamma_h^-$ ], according to the choice (7) or (8). Discrete boundary condition operator can be expressed by:

$\mathcal{B}_h : \bar{S}(\Omega_h) \rightarrow S(\partial\Omega_h)$  such that  $\mathcal{B}_h(u_h) = \tilde{u}(B)$  according to the Eq. (13),

and the respective discrete right-hand side is a grid function  $g_h \in S(\partial\Omega_h)$  such that  $g_h(G) = g(B)$  according to the Eq. (13). With this notation, we can write the linear system on the grid with spatial step  $h$  in the following compact form:

$$\begin{aligned} L_h(\beta_h, u_h) &= f_h \\ [\beta_h, u_h]_h^- &= g_h^- \\ [\beta_h, u_h]_h^+ &= g_h^+ \\ \mathcal{B}(u_h) &= g_h \end{aligned} \tag{40}$$

In order to describe the multigrid algorithm, we first introduce the extension operator and the transfer (restriction and interpolation) operators.

#### 4.2.1 Extension operator

Let us consider the whole domain  $\Omega$  (the argument can be easily repeated with the two subdomains  $\Omega^-$  and  $\Omega^+$ ). This domain is defined by a level-set function  $\phi$  and it defines a set of inner grid points  $\Omega_h$  and a set of ghost points  $\partial\Omega_h$ . Let us suppose we know a grid function  $\omega_h$  only on grid nodes of  $\partial\Omega_h$  (i.e.  $\omega_h \in S(\partial\Omega_h)$ ) and we want to extend  $\omega_h$  in the whole domain  $D_h \setminus \Omega_h$ , namely we want to obtain a new grid function  $\omega_h^{ext} \in S(D_h \setminus \Omega_h)$ . The function  $\omega_h^{ext}$  can be obtained by extrapolating  $\omega_h$  constant along the normal direction to  $\partial\Omega$ , i.e. solving the transport equation

$$\frac{\partial \omega}{\partial \tau} + \nabla \omega \cdot \mathbf{n} = 0 \tag{41}$$

for a few steps of a fictitious time  $\tau$ , where  $\omega = \omega_h$  in  $\partial\Omega_h$ , and  $\mathbf{n} \equiv (n_x, n_y) = \nabla \phi / |\nabla \phi|$  is the unit normal vector. The procedure is analogous to the one presented in [15] for the case of continuous coefficients.

Finally, we can resume the extension process introducing an extension operator, which in practice depends only on the set of ghost point  $\partial\Omega_h$  and on the discretized signed distance function  $\phi_h$ . Therefore:

$$\mathcal{E}[\partial\Omega_h; \phi_h] : S(\partial\Omega_h) \longrightarrow S(D_h \setminus \Omega_h). \tag{42}$$

#### 4.2.2 Restriction operator

We want to define a suitable restriction operator:

$$\mathcal{I}_{2h}^h : S(Z_h) \rightarrow S(Z_{2h}), \text{ where } Z_h \subseteq D_h, \quad Z_{2h} = Z_h \cap D_{2h}.$$

We perform the usual full-weighting restriction away from the boundary/interface, while we modify the restriction for inner equations close to the boundary/interface and for the boundary conditions. We recall the full-weighting restriction operator (see [59, Ch. 2.3.3]):

$$\mathcal{I}_{2h}^h = \frac{1}{16} \begin{bmatrix} 1 & 2 & 1 \\ 2 & 4 & 2 \\ 1 & 2 & 1 \end{bmatrix}_{2h}^h. \quad (43)$$

In general, by the stencil notation

$$\mathcal{I}_{2h}^h = \begin{bmatrix} & \vdots & \vdots & \vdots & \\ \cdots & t_{-1,-1} & t_{-1,0} & t_{-1,1} & \cdots \\ \cdots & t_{0,-1} & t_{0,0} & t_{0,1} & \cdots \\ \cdots & t_{1,-1} & t_{1,0} & t_{1,1} & \cdots \\ & \vdots & \vdots & \vdots & \end{bmatrix}_{2h}^h$$

we will intend the restriction operator  $\mathcal{I}_{2h}^h$  defined by:

$$\mathcal{I}_{2h}^h w_h(x, y) = \sum_{(i,j) \in R_k} t_{i,j} w_h(x + jh, y + ih),$$

where only a finite number of coefficients  $t_{i,j}$  is different from zero, and  $R_k \equiv \{-k, \dots, k\}^2$  for some positive integer  $k$ . In practice,  $k = 1$  allows second order restriction operator.

Following the same technique of [15], we modify the restriction operator when we are close to the interface/boundary in such a way we only use values coming from the same side of the interface/boundary. The modified restriction operator acting on a general subset  $Z_h \subseteq D_h$  is therefore defined as follows. Let  $(x, y) \in Z_{2h}$  and let  $\mathcal{N}(x, y) = \{(x + jh, y + ih) : j, i = -1, 0, 1\}$  be the neighborhood of  $(x, y)$ . We define  $\mathcal{T}$  as the maximum full rectangle with vertices belonging to  $\mathcal{N}(x, y)$  and such that  $\mathcal{T} \cap D_h \subseteq Z_h$  (see Fig. 7, where  $Z_h = \Omega_h^-$ ). The stencil used in  $(x, y)$  to transfer  $w_h$  to a coarser grid depends on the size of  $\mathcal{T}$ . In particular, if  $\mathcal{T} \cap D_h$  is a  $3 \times 3$  point stencil (i.e.  $\mathcal{N}(x, y) \subseteq Z_h$ ), then we can use the standard full-weighting stencil (43). Now let  $\mathcal{T} \cap D_h$  be a  $3 \times 2$  point stencil (the case  $2 \times 3$  is similar). Without loss of generality, we can suppose that the vertices of  $\mathcal{T}$  are  $(x + jh, y + ih)$ , with  $j \in \{-1, 0\}$ ,  $i \in \{-1, 1\}$ . In this case, the restriction operator is:

$$\left( I_{2h}^h w_h \right) (x, y) = \frac{1}{16} \begin{bmatrix} 2 & 2 & 0 \\ 4 & 4 & 0 \\ 2 & 2 & 0 \end{bmatrix}_{2h}^h (x, y), \quad (44)$$

while, if  $\mathcal{T}$  is a  $2 \times 2$  point stencil, with vertex  $(x + jh, y + ih)$ ,  $j, i \in \{-1, 0\}$ , the restriction operator is:

$$\left( I_{2h}^h w_h \right) (x, y) = \frac{1}{16} \begin{bmatrix} 0 & 0 & 0 \\ 4 & 4 & 0 \\ 4 & 4 & 0 \end{bmatrix}_{2h}^h (x, y), \quad (45)$$

These three cases are summarized in Fig. 7 (where  $Z_h = \Omega_h^-$ ).

The restriction of the boundary/interface conditions is performed similarly, provided extending the defect of the boundary/interface conditions away from the boundary/interface (by the procedure described in Sec. 4.2.1) and then performing the same restriction procedure, using only the values coming from the same side of the boundary/interface. The procedure will be described in detail in Sec. 4.2.4.

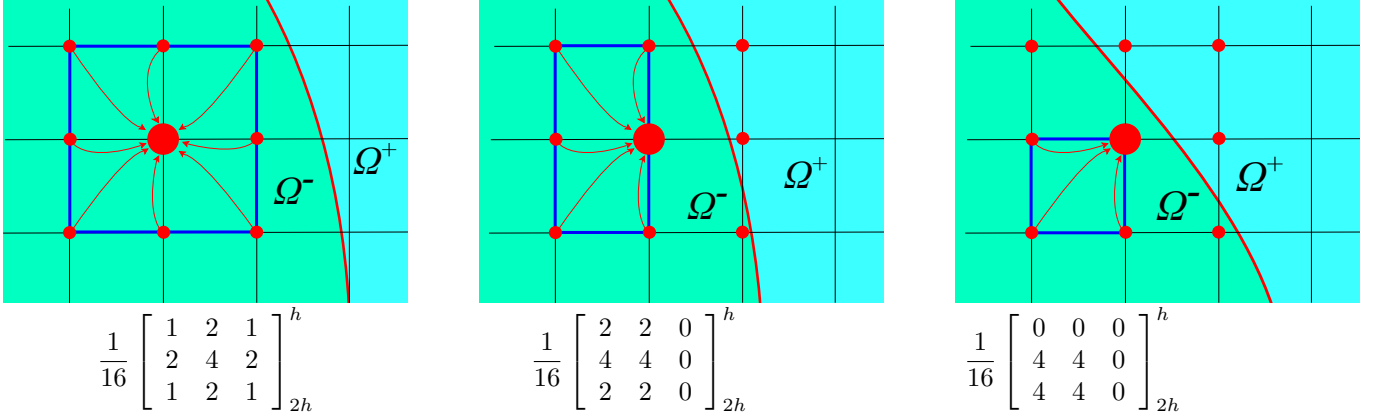


Fig. 7: Top: nine point stencil  $\mathcal{N}(x, y)$  (circles) and the boundary of the rectangle  $\mathcal{T}$  (bold line). The bold circle is on both the coarser and finer grids, while the smaller circles are only on the finer grid. The arrows represent the action of the restriction operators. Bottom: the respective stencils in matrix form used by the restriction operator.

### 4.2.3 Interpolation operator

The interpolation operator of the multigrid algorithm acts on the error, which is continuous across the boundary/interface. Therefore, we do not need to modify the stencil for particular cases and we are allowed to use the standard linear interpolation operator:

$$\mathcal{I}_h^{2h} = \frac{1}{4} \begin{bmatrix} 1 & 2 & 1 \\ 2 & 4 & 2 \\ 1 & 2 & 1 \end{bmatrix} \begin{matrix} h \\ 2h \\ h \end{matrix}. \quad (46)$$

### 4.2.4 Two-Grid Correction scheme

Let us suppose we have an exact solver  $\mathcal{S}$  of the linear system (40) for a grid with an arbitrary spatial step  $h$ :

$$u_h = \mathcal{S}(\beta_h, f_h^-, f_h^+, g_h^-, g_h^+, g_h).$$

Now, in order to describe the multigrid technique to solve the linear system (40), it is sufficient to describe the TGCS (Two-Grid Correction Scheme), since any other multigrid algorithm (such as for example  $V$ -cycle,  $W$ -cycle, Full Multigrid) can be easily derived from it (see [59, Ch. 2.4, 2.6] for more details). The TGCS consists into the following algorithm:

1. Set initial guess  $u_h = 0$ ;
2. Relax  $\nu_1$  times (by the Algorithm 1) on the grid with spatial step  $h$
3. Compute the following defects:

$$\begin{aligned} r_h^{\Omega^-} &= f_h^- - L_h^-(\beta_h^-, u_h^-) \\ r_h^{\Omega^+} &= f_h^+ - L_h^+(\beta_h^+, u_h^+) \\ r_h^{\Gamma^-} &= g_h^- - [\beta_h, u_h]_h^- \\ r_h^{\Gamma^+} &= g_h^+ - [\beta_h, u_h]_h^+ \\ r_h^{\partial\Omega} &= g_h - \mathcal{B}(u_h) \end{aligned}$$

4. Extend the defects  $r_h^{\Gamma^-}$ ,  $r_h^{\Gamma^+}$  and  $r_h^{\Gamma}$  using the extension operator defined in (42):

$$\begin{aligned} r_h^{\Gamma^-,ext} &= \mathcal{E}[\Gamma_h^-; \phi_h^\Gamma](r_h^{\Gamma^-}), \\ r_h^{\Gamma^+,ext} &= \mathcal{E}[\Gamma_h^+; -\phi_h^\Gamma](r_h^{\Gamma^+}), \\ r_h^{\partial\Omega,ext} &= \mathcal{E}[\partial\Omega_h; \phi_h](r_h^{\partial\Omega}). \end{aligned}$$

5. Transfer these defects to a coarser grid with spatial step  $2h$  by the *restriction operator* defined in Sec. 4.2.2:

$$\begin{aligned} r_{2h}^{\Omega^-} &= I_{2h}^h(r_h^{\Omega^-}) \\ r_{2h}^{\Omega^+} &= I_{2h}^h(r_h^{\Omega^+}) \\ r_{2h}^{\Gamma^-} &= I_{2h}^h(r_h^{\Gamma^-,ext}) \\ r_{2h}^{\Gamma^+} &= I_{2h}^h(r_h^{\Gamma^+,ext}) \\ r_{2h}^{\partial\Omega} &= I_{2h}^h(r_h^{\partial\Omega,ext}) \end{aligned}$$

6. Solve the residual problem in the coarser grid

$$e_{2h} = \mathcal{S}(\beta_{2h}, r_{2h}^{\Omega^-}, r_{2h}^{\Omega^+}, r_{2h}^{\Gamma^-}, r_{2h}^{\Gamma^+}, r_{2h}^{\partial\Omega})$$

7. Transfer the error to the finer grid by the interpolation operator (46):

$$e_h = I_h^{2h}(e_{2h})$$

8. Correct the fine-grid approximation

$$u_h := u_h + e_h$$

9. Relax  $\nu_2$  times (by the Algorithm 1) on the grid with spatial step  $h$ .

As mentioned above, the other multigrid algorithms are based on the recursive application of the TGCS. For example, the  $V$ -cycle algorithm is obtained by substituting the exact solver of step 6 with the application of the TGCS in the coarser grid. The recursive procedure continues until a suitable coarse grid is reached, where the exact solver is employed.

One multigrid iteration consists of an entire  $V$ -cycle. Iterations are performed until a suitable tolerance is satisfied, chosen in such a way the algebraic error (due to this stopping criterion) is negligible with respect to the discretization error.

## 5 Numerical tests

In this section we perform different numerical tests to show the second-order accuracy in the solution and its gradient and the efficiency of the multigrid. In detail, Examples 1 (circular domains) and 2 (flower-shaped domains) show the accuracy of the discretization. The tolerance for the stopping criterion of the multigrid is small enough in order to make the error of the iterative scheme negligible with respect to the one associated with the discretization error. Therefore, the error of the numerical results is (almost) entirely due to the discretization error, which decays with second order accuracy. Although second order accuracy in both the solution and the gradient is achieved, large errors are observed when  $\beta^- \gg \beta^+$  due to the artificiality of the numerical tests, as demonstrated in Example 3 (where more realistic data is chosen). Example 4 is related to the efficiency of the multigrid for high-jump coefficients. In order to avoid numerical instability associated with the machine precision, we test the multigrid efficiency on the homogeneous problem (starting with an initial guess different from zero) and analyze the convergence factor towards the exact (null) solution.



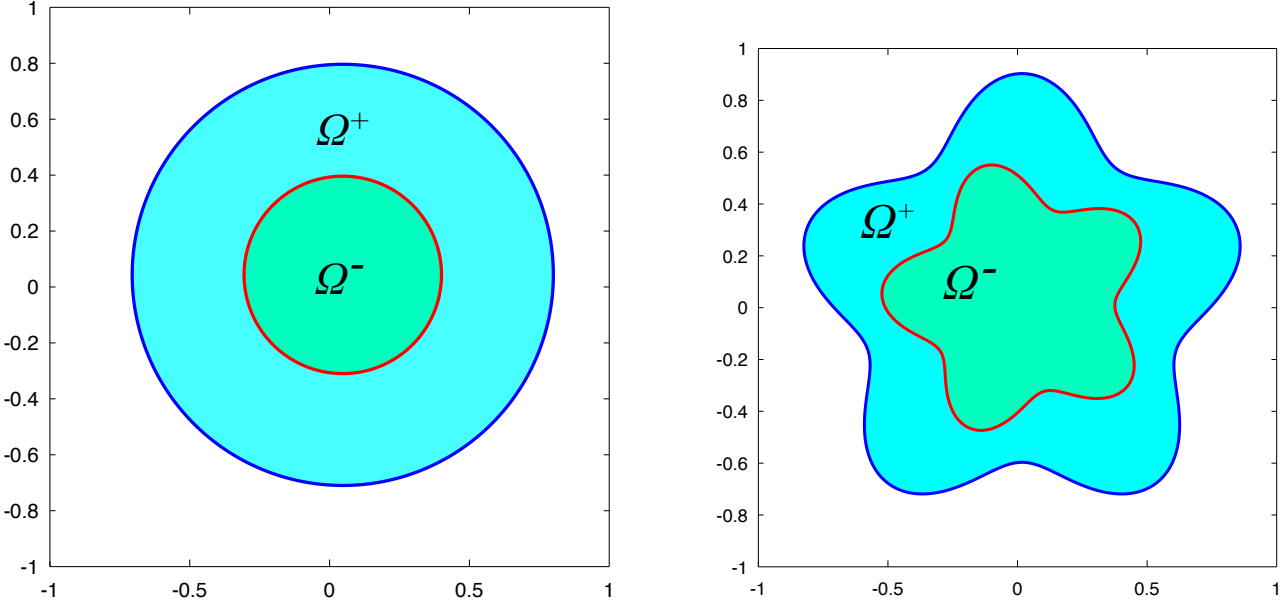


Fig. 8: Domains  $\Omega^-$  and  $\Omega^+$  of the Examples 5.1 and 5.3 (left), 5.2 and 5.4 (right).

### 5.1 Example 1: circular domains

Let us consider the model problem (1) with the following data:

$$\begin{aligned} \phi^\Gamma(x, y) &= \sqrt{(x - x_0)^2 + (y - y_0)^2} - R_1, \\ \phi(x, y) &= \sqrt{(x - x_0)^2 + (y - y_0)^2} - R_2, \\ \beta^- &= 10^6 + 10^5 \sin(\pi x) \cos(3\pi y), \quad \beta^+ = 1 + 0.5 \sin(2\pi x) \cos(4\pi y) \end{aligned} \quad (47)$$

or

$$\beta^- = 1 + 0.5 \sin(2\pi x) \cos(4\pi y), \quad \beta^+ = 10^6 + 10^5 \sin(\pi x) \cos(3\pi y). \quad (48)$$

Functions  $f^\pm$ ,  $g_D$ ,  $g_N$  and  $g$  are chosen in such a way the exact solution is the following:

$$u^- = \sin(4\pi x) \cos(6\pi y), \quad u^+ = \cos(2\pi x) \sin(3\pi y).$$

We choose  $x_0 = \sqrt{2}/30$ ,  $y_0 = \sqrt{3}/40$ ,  $R_1 = 0.353$  and  $R_2 = 0.753$ . The domain is represented in Fig. 8 (left side). We perform one test with (51) and one test with (48). In Tables 1 and 2 we list the errors of the solution and its gradient in the  $L^1$  and  $L^\infty$  norms, while Fig. 9 shows the related bestfit lines. Second order accuracy is attained in both the solution and its gradient, and the errors are almost aligned with the best-fit line, highlighting the robustness of the method even with variable coefficients (with jump ratio up to one million).

We observe in Table 1 that, although second order accuracy is observed, very large errors are actually displayed compared to the exact solution, even for a reasonable number of grid points. This phenomenon is attributable to the artificial test rather than to an issue of the numerical method, and it is present only when the coefficient  $\beta^-$  of the internal domain  $\Omega^-$  is much larger than the coefficient  $\beta^+$  of the domain  $\Omega^+$  (in fact it does not appear in Table 2). A similar behavior is observed, for example, in [47]. A possible explanation is given in Appendix 2. We remind that  $f^\pm$ ,  $g_D$ ,  $g_N$  and  $g$  are defined artificially as a consequence of the chosen exact solution to test the second order accuracy of the method, and leading (when  $\beta^- \gg \beta^+$ ) to high-jump data (such as  $f$ ) and then to

large errors compared to the exact solution. In real-life applications,  $f^\pm$ ,  $g_D$ ,  $g_N$  and  $g$  are set up according to the specific application and then this phenomenon is not present. The numerical test proposed in (5.3) supports this latter statement.

Table 1: Example 5.1. Accuracy order in the solution (top) and in the gradient (bottom) for the case (51).

No. of points	$L^1$ error of $u$	order	$L^\infty$ error of $u$	order
$32 \times 32$	$8.34 \cdot 10^3$	-	$7.70 \cdot 10^4$	-
$64 \times 64$	$2.07 \cdot 10^3$	2.01	$1.85 \cdot 10^4$	2.06
$128 \times 128$	$5.79 \cdot 10^2$	1.84	$5.10 \cdot 10^3$	1.86
$256 \times 256$	$1.46 \cdot 10^2$	1.99	$1.28 \cdot 10^3$	2.00
No. of points	$L^1$ error of $ \nabla u $	order	$L^\infty$ error of $ \nabla u $	order
$32 \times 32$	$1.46 \cdot 10^5$	-	$3.90 \cdot 10^5$	-
$64 \times 64$	$3.49 \cdot 10^4$	2.06	$1.06 \cdot 10^5$	1.88
$128 \times 128$	$9.56 \cdot 10^3$	1.87	$2.96 \cdot 10^4$	1.84
$256 \times 256$	$2.39 \cdot 10^3$	2.00	$7.45 \cdot 10^3$	1.99

Table 2: Example 5.1. Accuracy order in the solution (top) and in the gradient (bottom) for the case (48).

No. of points	$L^1$ error of $u$	order	$L^\infty$ error of $u$	order
$32 \times 32$	$4.40 \cdot 10^{-3}$	-	$1.22 \cdot 10^{-1}$	-
$64 \times 64$	$1.02 \cdot 10^{-3}$	2.11	$2.93 \cdot 10^{-2}$	2.06
$128 \times 128$	$3.29 \cdot 10^{-4}$	1.64	$7.61 \cdot 10^{-3}$	1.95
$256 \times 256$	$8.24 \cdot 10^{-5}$	2.00	$2.14 \cdot 10^{-3}$	1.83
No. of points	$L^1$ error of $ \nabla u $	order	$L^\infty$ error of $ \nabla u $	order
$32 \times 32$	$3.93 \cdot 10^{-1}$	-	$3.52 \cdot 10^0$	-
$64 \times 64$	$9.95 \cdot 10^{-2}$	1.98	$9.71 \cdot 10^{-1}$	1.86
$128 \times 128$	$2.63 \cdot 10^{-2}$	1.92	$2.80 \cdot 10^{-1}$	1.80
$256 \times 256$	$6.60 \cdot 10^{-3}$	1.99	$7.32 \cdot 10^{-2}$	1.93

## 5.2 Example 2: flower-shaped domains

Let us consider the general flower-shaped interface with parametric equations:

$$X(\vartheta) = r(\vartheta) \cos(\vartheta) + x_0,$$

$$Y(\vartheta) = r(\vartheta) \sin(\vartheta) + y_0,$$

with  $\vartheta \in [0, 2\pi]$  and  $r(\vartheta) = r_0 + r_1 \sin(\omega\vartheta)$ . Let us consider  $\omega = 5$ . The level-set representation of this interface is:

$$\text{flower}_0(r_0, r_1, x_0, y_0; x, y) = r - r_0 - r_1 \frac{(y - y_0)^5 + 5(x - x_0)^4(y - y_0) - 10(x - x_0)^2(y - y_0)^3}{r^5}.$$

where  $r = \sqrt{(x - x_0)^2 + (y - y_0)^2}$ . A rotated version (counter-clockwise by an angle  $\vartheta_0$ ) of this interface is obtained by considering the following level-set function:

$$\text{flower}(r_0, r_1, x_0, y_0, \vartheta_0; x, y) = \text{flower}_0(r_0, r_1, x_0, y_0; x^*, y^*),$$

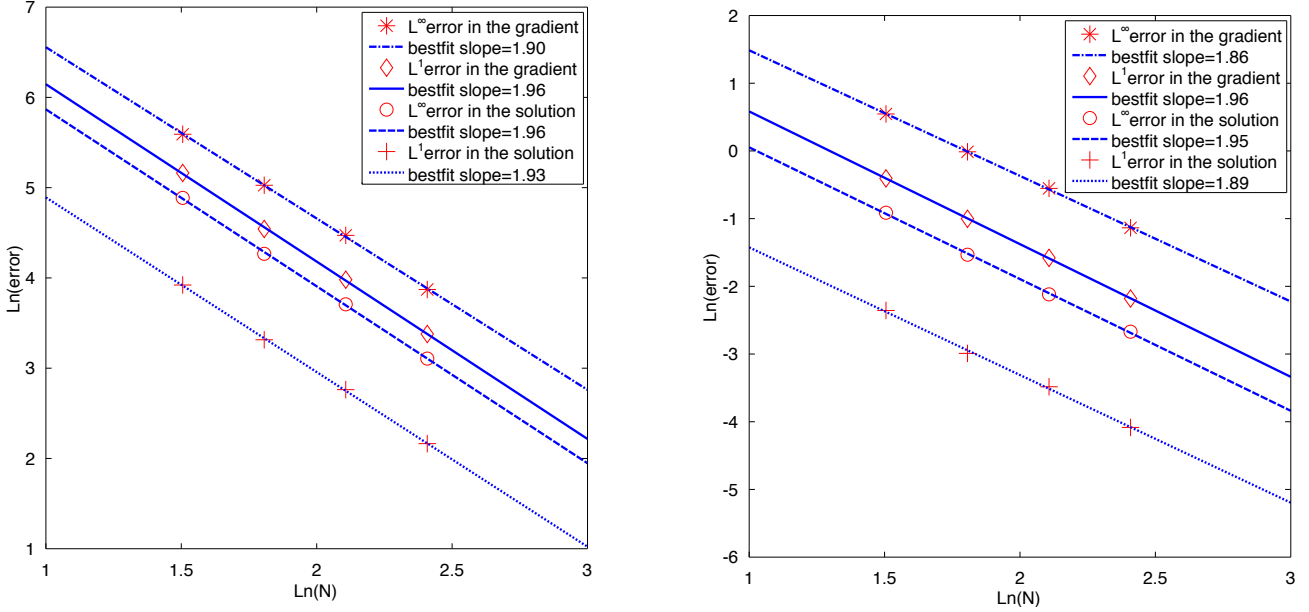


Fig. 9: Example 5.1. Bestfit lines of the errors in the solution and in the gradient (Tables 1 and 2) in both the  $L^1$  and  $L^\infty$  norms. Left:  $\beta^-$  and  $\beta^+$  are given by (51); Right:  $\beta^-$  and  $\beta^+$  are given by (48).

where

$$\begin{aligned} x^* &= \cos(\vartheta_0)x - \sin(\vartheta_0)y, \\ y^* &= \sin(\vartheta_0)x + \cos(\vartheta_0)y. \end{aligned}$$

Let us consider the model problem (1) with the following data:

$$\begin{aligned} \phi^\Gamma(x, y) &= \text{flower}(0.45, 1/12, 0.01\sqrt{3}, 0.02\sqrt{2}, -\pi/12; x, y), \\ \phi(x, y) &= \text{flower}(0.75, 1/8, 0.01\sqrt{3}, 0.02\sqrt{2}, 0; x, y), \\ \beta^- &= 10^6 + 10^5 \sin(\pi x) \cos(3\pi y), \quad \beta^+ = 1 + 0.5 \sin(2\pi x) \cos(4\pi y) \end{aligned} \quad (49)$$

or

$$\beta^- = 1 + 0.5 \sin(2\pi x) \cos(4\pi y), \quad \beta^+ = 10^6 + 10^5 \sin(\pi x) \cos(3\pi y). \quad (50)$$

Functions  $f^\pm$ ,  $g_D$ ,  $g_N$  and  $g$  are chosen in such a way the exact solution is the following:

$$u^- = \sin(4\pi x) \cos(6\pi y), \quad u^+ = \cos(2\pi x) \sin(3\pi y),$$

The domain is represented in Fig. 8 (right side). We perform one test with (49) and one test with (50). In Tables 3 and 4 we list the errors of the solution and its gradient in the  $L^1$  and  $L^\infty$  norms. Fig. 10 shows the related bestfit lines.

As in the previous case, also in the presence of complex interface/boundary the method is robust and second order accurate in both the solution and its gradient. The phenomenon of large errors in Table 3 is similar to the one observed in Example 1 and the explanation is given in Appendix 2. The numerical test (5.3) demonstrates that this issue is related with the artificial aspect of the numerical test rather than with the discretization method.

Table 3: Example 5.2. Accuracy order in the solution (top) and in the gradient (bottom) for the case (49).

No. of points	$L^1$ error of $u$	order	$L^\infty$ error of $u$	order
$32 \times 32$	$6.99 \cdot 10^3$	-	$5.77 \cdot 10^4$	-
$64 \times 64$	$1.17 \cdot 10^3$	2.58	$9.27 \cdot 10^3$	2.64
$128 \times 128$	$5.69 \cdot 10^2$	1.04	$4.32 \cdot 10^3$	1.10
$256 \times 256$	$7.61 \cdot 10^1$	2.90	$5.65 \cdot 10^2$	2.93
No. of points	$L^1$ error of $ \nabla u $	order	$L^\infty$ error of $ \nabla u $	order
$32 \times 32$	$1.23 \cdot 10^5$	-	$5.02 \cdot 10^5$	-
$64 \times 64$	$1.95 \cdot 10^4$	2.65	$8.69 \cdot 10^4$	2.53
$128 \times 128$	$9.30 \cdot 10^3$	1.07	$4.38 \cdot 10^4$	0.99
$256 \times 256$	$1.23 \cdot 10^3$	2.92	$6.26 \cdot 10^3$	2.80

Table 4: Example 5.2. Accuracy order in the solution (top) and in the gradient (bottom) for the case (50).

No. of points	$L^1$ error of $u$	order	$L^\infty$ error of $u$	order
$32 \times 32$	$6.63 \cdot 10^{-3}$	-	$2.51 \cdot 10^{-1}$	-
$64 \times 64$	$2.49 \cdot 10^{-3}$	1.41	$8.18 \cdot 10^{-2}$	1.62
$128 \times 128$	$5.02 \cdot 10^{-4}$	2.31	$1.66 \cdot 10^{-2}$	2.30
$256 \times 256$	$1.28 \cdot 10^{-4}$	1.98	$4.03 \cdot 10^{-3}$	2.04
No. of points	$L^1$ error of $ \nabla u $	order	$L^\infty$ error of $ \nabla u $	order
$32 \times 32$	$6.70 \cdot 10^{-1}$	-	$4.30 \cdot 10^0$	-
$64 \times 64$	$1.91 \cdot 10^{-1}$	1.81	$1.19 \cdot 10^0$	1.86
$128 \times 128$	$4.64 \cdot 10^{-2}$	2.04	$3.31 \cdot 10^{-1}$	1.84
$256 \times 256$	$1.18 \cdot 10^{-2}$	1.97	$1.23 \cdot 10^{-1}$	1.43

### 5.3 Example 3: accuracy test with more realistic data $f^\pm$ , $g_D$ , $g_N$ and $g$

In this test we show that the large errors present in Tables 1 and 3 are actually a consequence of the artificial aspect of the numerical tests rather than an issue of the discretization method itself. To this purpose, we choose more realistic values for the right-hand sides  $f^\pm$ ,  $g_D$ ,  $g_N$  and  $g$ , rather than computing them by the exact solution (which can lead to high jumps in  $f$  and then to large numerical errors). In absence of the exact solution, we compute the errors by comparing the numerical solution with a reference solution rather than with the exact solution (which is not available here). In this test, the reference solution is the numerical solution with a sufficiently large number of grid points ( $1024 \times 1024$  in our case). The reference gradient of the solution is computed by standard central difference schemes on the reference solution.

Let us consider the model problem (1) with the following data:

$$\begin{aligned}
 \phi^\Gamma(x, y) &= \sqrt{(x - x_0)^2 + (y - y_0)^2} - R_1, \\
 \phi(x, y) &= \sqrt{(x - x_0)^2 + (y - y_0)^2} - R_2, \\
 \beta^- &= 10^6 + 10^5 \sin(\pi x) \cos(3\pi y), \quad \beta^+ = 1 + 0.5 \sin(2\pi x) \cos(4\pi y), \\
 f^- &= \sin(4\pi x) \cos(6\pi y), \quad f^+ = \cos(2\pi x) \sin(3\pi y), \\
 g_D &= g_N = g = 0.
 \end{aligned} \tag{51}$$

As in Example 5.1, we choose  $x_0 = \sqrt{2}/30$ ,  $y_0 = \sqrt{3}/40$ ,  $R_1 = 0.353$  and  $R_2 = 0.753$  (the domain is represented in Fig. 8, left side).

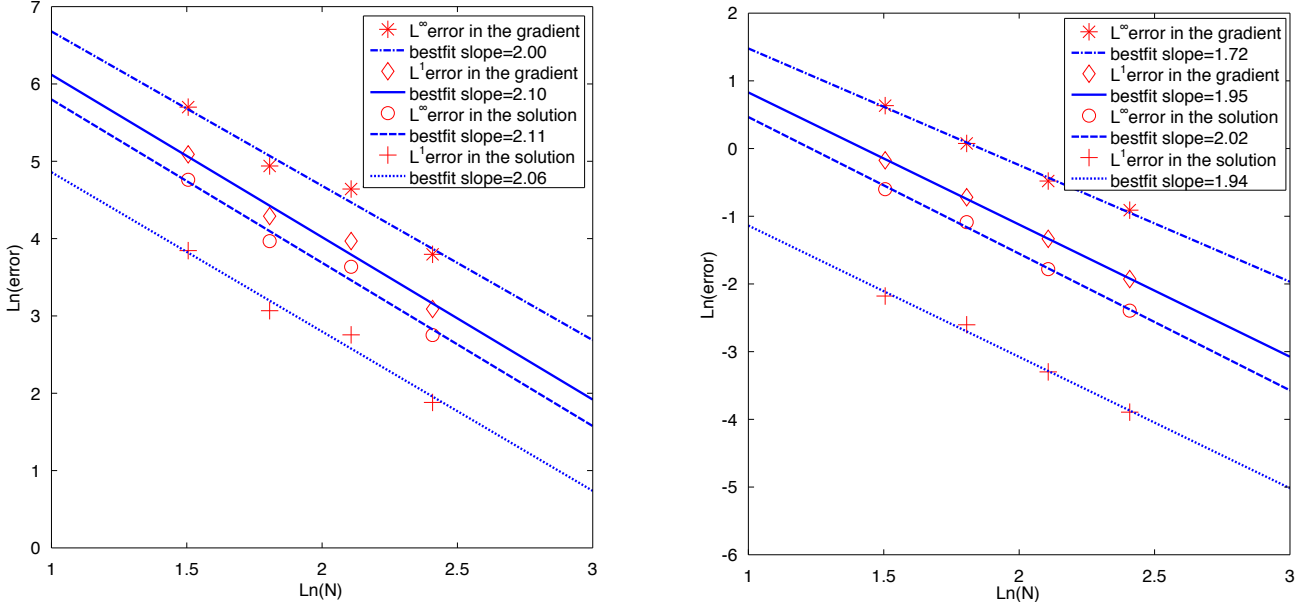


Fig. 10: Example 5.2. Bestfit lines of the errors in the solution and in the gradient (Tables 3 and 4) in both the  $L^1$  and  $L^\infty$  norms. Left:  $\beta^-$  and  $\beta^+$  are given by (49); Right:  $\beta^-$  and  $\beta^+$  are given by (49).

Table 5: Example 5.3. Accuracy order in the solution (top) and in the gradient (bottom).

No. of points	$L^1$ error of $u$	order	$L^\infty$ error of $u$	order
$32 \times 32$	$4.97 \cdot 10^{-5}$	-	$6.26 \cdot 10^{-4}$	-
$64 \times 64$	$8.43 \cdot 10^{-6}$	2.56	$1.05 \cdot 10^{-4}$	2.58
$128 \times 128$	$1.92 \cdot 10^{-6}$	2.13	$2.22 \cdot 10^{-5}$	2.24
$256 \times 256$	$3.63 \cdot 10^{-7}$	2.40	$4.60 \cdot 10^{-6}$	2.27
No. of points	$L^1$ error of $ \nabla u $	order	$L^\infty$ error of $ \nabla u $	order
$32 \times 32$	$1.88 \cdot 10^{-3}$	-	$1.30 \cdot 10^{-2}$	-
$64 \times 64$	$4.52 \cdot 10^{-4}$	2.06	$4.76 \cdot 10^{-3}$	1.45
$128 \times 128$	$1.10 \cdot 10^{-4}$	2.04	$1.06 \cdot 10^{-3}$	2.17
$256 \times 256$	$2.57 \cdot 10^{-5}$	2.09	$2.48 \cdot 10^{-4}$	2.09

As can be seen in Table 5, relative errors are now reasonable without compromising the second order accuracy in the solution and the gradient. Fig. 11 (left) shows the associated bestfit lines. The numerical solution (obtained with  $1024 \times 1024$  grid points) is displayed in Fig. 11 (right).

#### 5.4 Example 4: High-jump coefficients and multigrid efficiency

In this example we show that the asymptotic convergence factor of the multigrid algorithm does not depend on the jump of the coefficient nor on the size of the problem. In particular, we will see that the convergence factor is close to the one predicted by the Local Fourier Analysis for inner equations and detailed in Table 6. As we pointed out in Sec. 4.1.3, we know that more efficient smoothers than GS-LEX exist (such as GS-RB), but the goal of this

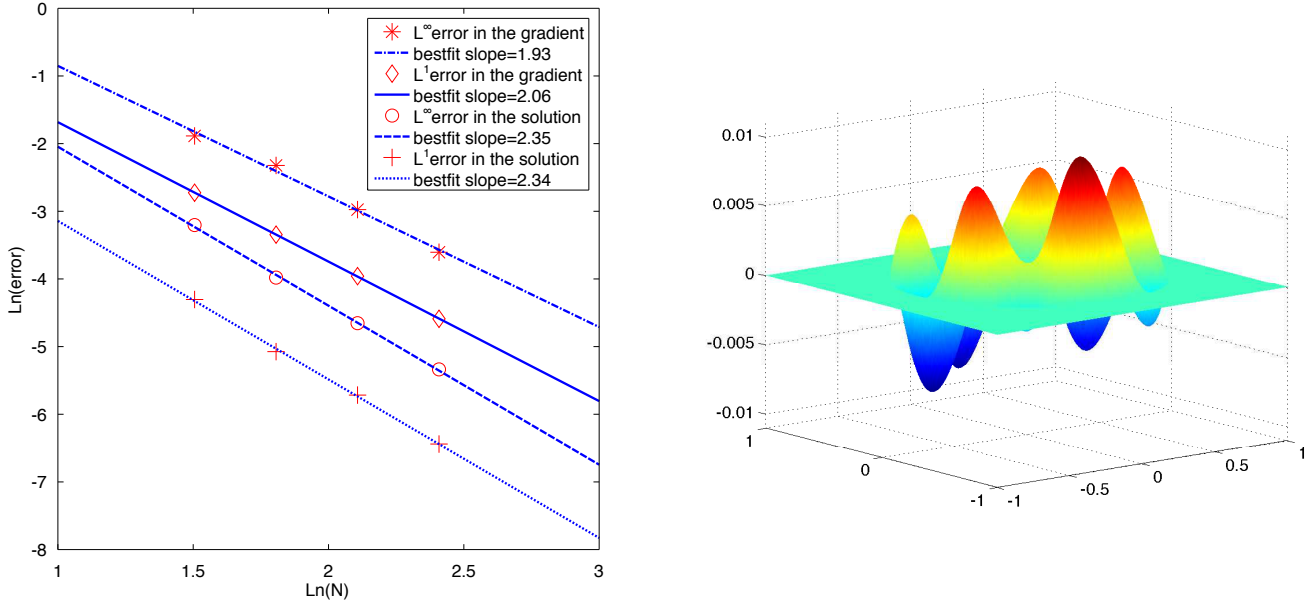


Fig. 11: Example 5.3. Left: bestfit lines of the errors in the solution and in the gradient (Table 5) in both the  $L^1$  and  $L^\infty$  norms. Right: numerical solution obtained with  $1024 \times 1024$  grid points.

work is to show that the optimal convergence factor is attained, regardless on the smoother adopted. The same argument holds for the multigrid algorithm: even if the Full Multigrid is more efficient, we limit ourselves to study the convergence factor for the W-cycle algorithm, in order to compare results with the well-known values of Table 6. However, we experienced that the convergence factor is close to the optimal one in the first few cycles of the entire algorithm (say the first ten), while it slightly degrades when reaching asymptotic convergence.

Table 6: Predicted convergence factor  $\rho_{loc}$  by LFA for GS-LEX and FW restriction operator (see, for instance, [59, Ch. 4.6.1]).

$\nu = \nu_1 + \nu_2$	1	2	3	4
$\rho_{loc}$	0.400	0.193	0.119	0.084

Let us recall that we estimate the asymptotic convergence factor as:

$$\rho = \lim_{m \rightarrow \infty} \rho^{(m)} = \lim_{m \rightarrow \infty} \frac{\|r_h^{(m)}\|_\infty}{\|r_h^{(m-1)}\|_\infty},$$

where  $r_h = (r_h^{\Omega^-}, r_h^{\Omega^+}, r_h^{\Gamma^-}, r_h^{\Gamma^+}, r_h^\Gamma)$ . In practice, we compute  $\rho^{(m)}$  until the following stopping criterion is satisfied:

$$\frac{|\rho^{(m)} - \rho^{(m-1)}|}{\rho^{(m)}} < 10^{-3}. \quad (52)$$

We compare this convergence factor with the average convergence factor of the first ten W-cycle iterations, computed

as follows:

$$\bar{\rho} = \sqrt[9]{\prod_{m=2}^{10} \rho^{(m)}}. \quad (53)$$

In this example, we use the same geometry as in Example 5.2 (namely the flower-shaped domains), with coefficients:

$$\beta^- = 10^p, \quad \beta^+ = 1.$$

We solve the homogeneous problem (starting with an initial guess different from zero), namely the Problem (1) with  $f^\pm = g_D = g_N = g = 0$ , in order to avoid numerical instability associated with the machine precision. We use the  $W$ -cycle algorithm with  $\nu_1 = 2$  pre-smoothing and  $\nu_2 = 1$  post-smoothing relaxations (therefore  $\nu = 3$  in Table 6), and with a coarsest grid of  $16 \times 16$  grid points. Tables 7 and 8 show the estimated convergence factors for different numbers of grid points and jumps in the coefficient. As we can see from Tables 7 and 8, the average convergence factor of the method is almost comparable with the result predicted by the Local Fourier Analysis, and then the method is very effective on such problems. We observe that in some cases the convergence factor is even less than the predicted one. A possible explanation for this phenomenon lies in the choice of the parameter  $\lambda$  and  $\delta$  in Eq. (39). In fact, this choice is performed at every level of the multigrid, even for coarser grids, where the choice  $\delta = 5h$  leads to perform the extra-relaxation steps on the whole domain, and then the actual value of iteration steps  $\nu = \nu_1 + \nu_2$  is higher than three on those coarser levels. This phenomenon improves the overall efficiency of the multigrid with some extra computational cost.

Finally, it is worth to observe that if the choice (34)–(37) is performed in the opposite way (i.e. (35),(37) if  $\beta^+(I) > \beta^-(I)$ , and (34),(36) otherwise), then the convergence factor degrades to  $\rho \approx 1$  (not shown).

Table 7: Example 5.4. Asymptotic convergence factor, computed with the stop criterion (52) ( $\nu = \nu_1 + \nu_2 = 3$ ).

$N^2$	$p$	-9	-7	-5	-3	-1
$32^2$		0.0875	0.0875	0.0875	0.0872	0.1019
$64^2$		0.1723	0.1723	0.1722	0.1553	0.1103
$128^2$		0.1616	0.1616	0.1616	0.1616	0.1616
$N^2$	$p$	1	3	5	7	9
$32^2$		0.2302	0.2411	0.2411	0.2411	0.2411
$64^2$		0.2176	0.2442	0.2445	0.2445	0.2445
$128^2$		0.1617	0.1618	0.1947	0.1947	0.1947

## 6 Conclusion

A ghost-point finite difference method to solve elliptic equations with discontinuous coefficients is presented. The method is second order accurate both in the solution and in the gradient, and therefore it is suitable for real-life applications that require additional accuracy also in the gradient, such as Stefan problems or incompressible Navier-Stokes equations. The accuracy order is not influenced by high-jump coefficients and can be straightforwardly increased by using a higher order interpolation procedure on the interface and boundary. The linear system arising from the discretization is solved by a proper multigrid approach, whose convergence factor is close to the optimal one achieved by the Local Fourier Analysis for rectangular domain and it is not affected by high-jump coefficients. Numerous applications may benefit from the higher accuracy of this method and the efficiency of the multigrid

Table 8: Example 5.4. Average convergence factor for the first ten  $W$ -cycle iterations, computed by the formula (53) ( $\nu = \nu_1 + \nu_2 = 3$ ).

$N^2$	$p$	-9	-7	-5	-3	-1
$32^2$		0.0776	0.0776	0.0776	0.0773	0.0486
$64^2$		0.0930	0.0930	0.0930	0.0930	0.1107
$128^2$		0.1544	0.1544	0.1544	0.1544	0.1544
$N^2$	$p$	1	3	5	7	9
$32^2$		0.1563	0.1586	0.1585	0.1585	0.1585
$64^2$		0.0931	0.1027	0.1029	0.1029	0.1029
$128^2$		0.1543	0.1543	0.1544	0.1544	0.1544

solver, such as those mentioned in the introduction, especially for the 3D case. Extension of the method to the case of adaptive Cartesian grids [55] and High Performance Computing [12] is part of our future work.

## Acknowledgment

The work of A. Coco has been partially supported by the London Mathematical Society Computer Science Small Grants - Scheme 7. The work of G. Russo was supported in part by ITN-ETN Horizon 2020 Project ModCompShock, Modeling and Computation on Shocks and Interfaces, Project Reference 642768.

## Appendix 1: Upper bounds for 2D interpolation coefficients

In this appendix we prove the equations (24), (25), (27) and (28). Let  $St_9$  be the  $3 \times 3$  point stencil of Fig. 12 (we assume that  $G$  is at the bottom left of the stencil, since the other three cases are analogous)

$$St_9 = \{G + h(i, j) : (i, j) \in \{0, 1, 2\}^2\},$$

and  $I \equiv (x_I, y_I)$  be a point such that  $x_G \leq x_I \leq x_G + h$ ,  $y_G \leq y_I \leq y_G + h$ . Let  $u_{ij}$ ,  $(i, j) \in \{0, 1, 2\}^2$ , be a grid function defined on the stencil  $St_9$  and  $\tilde{u}_h$  be the biquadratic interpolant of  $u_{ij}$  on the stencil  $St_9$ . Let  $\vartheta_x = \frac{x_I - x_G}{h}$  and  $\vartheta_y = \frac{y_I - y_G}{h}$ . Observe that  $0 \leq \vartheta_x, \vartheta_y \leq 1$ . After some algebra, we have

$$\tilde{u}_h(I) = \sum_{0 \leq i, j \leq 2} c_i^x c_j^y u_{ij}, \quad \frac{\partial \tilde{u}_h(I)}{\partial x} = \sum_{0 \leq i, j \leq 2} c_i^x c_j^y u_{ij}, \quad \frac{\partial \tilde{u}_h(I)}{\partial y} = \sum_{0 \leq i, j \leq 2} c_i^x c_j^y u_{ij},$$

where

$$\begin{aligned} (c_0^x, c_1^x, c_2^x) &= \left( \frac{(1 - \vartheta_x)(2 - \vartheta_x)}{2}, \vartheta_x(2 - \vartheta_x), \frac{(\vartheta_x - 1)\vartheta_x}{2} \right), \\ (c_0^y, c_1^y, c_2^y) &= \left( \frac{(1 - \vartheta_y)(2 - \vartheta_y)}{2}, \vartheta_y(2 - \vartheta_y), \frac{(\vartheta_y - 1)\vartheta_y}{2} \right), \\ (c_0^x, c_1^x, c_2^x) &= \frac{1}{h} \left( \vartheta_x - \frac{3}{2}, 2(1 - \vartheta_x), \vartheta_x - \frac{1}{2} \right), \\ (c_0^y, c_1^y, c_2^y) &= \frac{1}{h} \left( \vartheta_y - \frac{3}{2}, 2(1 - \vartheta_y), \vartheta_y - \frac{1}{2} \right). \end{aligned}$$



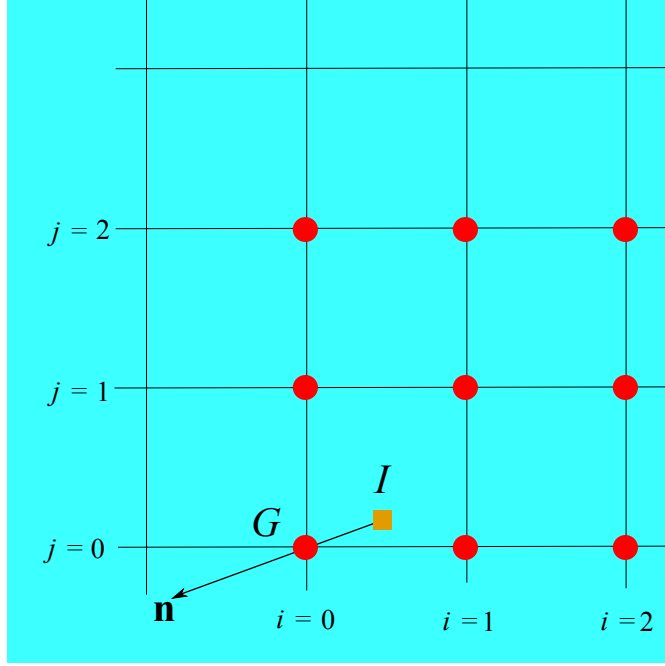


Fig. 12: Generic  $3 \times 3$  point stencil (circles) where a grid function  $u_{ij}$  is interpolated. Point  $G$  (ghost point) is at the bottom-left corner point. Point  $I$  (square point) is where the interpolation and its derivatives are evaluated. Unit vector  $\tilde{\mathbf{n}}$  represents the normal vector in Sec. 3 and then is almost parallel to  $G - I$ . In the Appendix, point  $I$  is in the bottom-left quadrant and  $\mathbf{n} = (n_x, n_y)$  is such that  $n_x, n_y \leq 0$ , but Eqs. (55), (56), (58), (59) are also valid in all the other three cases.

Therefore (observe that  $u_G = u_{00}$ ):

$$\frac{\partial \tilde{u}_h(I)}{\partial u_G} = c_0^x c_0^y = \frac{(1 - \vartheta_x)(2 - \vartheta_x)(1 - \vartheta_y)(2 - \vartheta_y)}{4}. \quad (54)$$

Since  $\vartheta_x, \vartheta_y \leq 1$ , we have:

$$\frac{\partial \tilde{u}_h(I)}{\partial u_G} \geq 0. \quad (55)$$

The supremum of (54) is attained for  $\vartheta_x = \vartheta_y = 0$ . Therefore:

$$\sup_{|G-I| \leq h} \frac{\partial \tilde{u}_h(I)}{\partial u_G} = 1. \quad (56)$$

Now, consider a generic unit vector  $\tilde{\mathbf{n}} = (n_x, n_y)$  pointing towards the bottom-left quadrant, i.e.  $n_x, n_y \leq 0$  and  $n_x^2 + n_y^2 = 1$ . Then:

$$\begin{aligned} \frac{\partial (\nabla \tilde{u}_h(I) \cdot \tilde{\mathbf{n}})}{\partial u_G} &= \frac{\partial}{\partial u_G} \left( \frac{\partial \tilde{u}_h(I)}{\partial x} n_x + \frac{\partial \tilde{u}_h(I)}{\partial y} n_y \right) = c_0^x c_0^y n_x + c_0^x c_0^y n_y \\ &= \frac{1}{h} \left( \frac{(3 - 2\vartheta_x)(1 - \vartheta_y)(2 - \vartheta_y)}{4} |n_x| + \frac{(1 - \vartheta_x)(2 - \vartheta_x)(3 - 2\vartheta_y)}{4} |n_y| \right). \end{aligned} \quad (57)$$

Since  $\vartheta_x, \vartheta_y \leq 1$ , we have:

$$\frac{\partial (\nabla \tilde{u}_h(I) \cdot \tilde{\mathbf{n}})}{\partial u_G} \geq 0. \quad (58)$$

The supremum of (57) is obtained for  $\vartheta_x = \vartheta_y = 0$  and  $|n_x| = |n_y| = \sqrt{2}/2$ . Therefore

$$\sup_{|G-I| \leq h} \frac{\partial (\nabla \tilde{u}_h(I) \cdot \tilde{\mathbf{n}})}{\partial u_G} = \frac{3}{\sqrt{2}h}. \quad (59)$$

Finally, we observe that the assumption that  $G$  is at the bottom-left corner does not lead the validity of Eqs. (55), (56), (58), (59), which are valid also in the three other cases.

## Appendix 2: Error upper bounds for 1D elliptic equations with discontinuous coefficients

In this appendix we compute an approximation of the upper bound for the error of 1D elliptic equations with discontinuous coefficients. The purpose of this section is to justify the large errors observed in Tables 1 and 3. Let us consider the 1D problem:

$$\left\{ \begin{array}{l} -\frac{d}{dx} \left( \beta^\pm \frac{du^\pm}{dx} \right) = f^\pm \text{ in } \Omega^\pm \\ \llbracket u \rrbracket = g_D \text{ on } x = -1 \text{ and } x = 1 \\ \llbracket \text{sign}(x) \beta \frac{du}{dx} \rrbracket = g_N \text{ on } x = -1 \text{ and } x = 1 \\ u = g \text{ on } x = -2 \text{ and } x = 2. \end{array} \right. \quad (60)$$

In this 1D problem we have  $\Omega^- = (-1, 1)$  and  $\Omega^+ = (-2, 2) \setminus \Omega^-$ . Let  $u_h$  be the discrete solution obtained by the 1D version of (40):

$$\begin{aligned} L_h(\beta_h, u_h) &= f_h \\ [\beta_h, u_h]_h^- &= g_h^- \\ [\beta_h, u_h]_h^+ &= g_h^+ \\ \mathcal{B}(u_h) &= g_h \end{aligned} \quad (61)$$

and  $e_h = u - u_h$ . Due to the linearity of the operators, we have:

$$\begin{aligned} L_h(\beta_h, e_h) &= L_h(\beta_h, u) - f_h \\ [\beta_h, e_h]_h^- &= [\beta_h, u]_h^- - g_h^- \\ [\beta_h, e_h]_h^+ &= [\beta_h, u]_h^+ - g_h^+ \\ \mathcal{B}(e_h) &= \mathcal{B}(u) - g_h \end{aligned} \quad (62)$$

Right-hand sides of Eq. (62) are the discretization errors of the operators. Therefore,  $e_h$  is a numerical approximation of the solution of the following problem:

$$\left\{ \begin{array}{l} -\frac{d}{dx} \left( \beta^\pm \frac{de^\pm}{dx} \right) = \beta^\pm C_1 h^2 \text{ in } \Omega^\pm \\ \llbracket e \rrbracket = C_2 h^3 \text{ on } x = -1 \text{ and } x = 1 \\ \llbracket \text{sign}(x) \beta \frac{de}{dx} \rrbracket = \max \{ \beta^+, \beta^- \} C_3 h^2 \text{ on } x = -1 \text{ and } x = 1 \\ e = C_4 h^3 \text{ on } x = -2 \text{ and } x = 2 \end{array} \right. \quad (63)$$

Let us assume for simplicity that  $\beta^+$  and  $\beta^-$  are two (possibly different) constants, and that the solution  $u$  of Eq. (60) and its derivatives up to order four are of  $O(1)$ , so that  $C_1 - C_4$  are constants of  $O(1)$ . Then, the exact

solutions of (63) are:

$$e^+(x) = -\frac{C_1 h^2}{2}(2 - |x|)^2 + \alpha(2 - |x|)h^2 + C_4 h^3, \quad e^-(x) = -\frac{C_1 h^2}{2}x^2 + (C_4 - C_2)h^3 + \alpha h^2, \quad (64)$$

with

$$\alpha = \frac{(\beta^+ + \beta^-)C_1 - \max\{\beta^+, \beta^-\} C_3}{\beta^+}.$$

From (64) we can infer that the error is in general  $O(\alpha h^2)$ . If  $\beta^+ > \beta^-$ , then  $\alpha$  is  $O(1)$ , while if  $\beta^- > \beta^+$  we observe that  $\alpha$  is  $O(\beta^-)$ . Finally, the error is  $O(h^2)$  when  $\beta^+ > \beta^-$ , and  $O(\beta^- h^2)$  when  $\beta^- > \beta^+$ . If  $\beta^- \gg \beta^+$  we observe that the error, although decays with second order of accuracy, may be very large for high value of  $h$ , and this explain the results of Tables 1 and 3.

## References

- [1] L. Adams and T. P. Chartier. New geometric immersed interface multigrid solvers. *SIAM Journal of Scientific Computing*, 25:1516–1533, 2004.
- [2] L. Adams and T. P. Chartier. A comparison of algebraic multigrid and geometric immersed interface multigrid methods for interface problems. *SIAM Journal of Scientific Computing*, 26:762–784, 2005.
- [3] L. Adams and Z. Li. The immersed interface/multigrid methods for interface problems. *Journal of Scientific Computing*, 24:463–479, 2002.
- [4] R. E. Alcouffe, A. Brandt, J. Dendy, J. E., and J. W. Painter. The multigrid method for the diffusion equation with strongly discontinuous coefficients. *Journal on Scientific and Statistical Computing*, 2:430–454, 1981.
- [5] P. Angot, C.-H. Bruneau, and P. Fabrie. A penalization method to take into account obstacles in incompressible viscous flows. *Numer. Math.*, 81, 1999.
- [6] I. Babuška. The finite element method for elliptic equations with discontinuous coefficients. *Computing*, 5:207–213, 1970.
- [7] J. Bramble and J. King. A finite element method for interface problems in domains with smooth boundaries and interfaces. *Adv. Comput. Math.*, 6:109–138, 1996.
- [8] W. L. Briggs, V. E. Henson, and S. F. McCormick. *A Multigrid Tutorial*. SIAM, 2000.
- [9] T. F. Chan and W. Wan. Robust multigrid methods for nonsmooth coefficient elliptic linear systems. *Journal of Computational and Applied Mathematics*, 123:323–352, 2000.
- [10] F. Chantalat, C.-H. Bruneau, C. Galusinski, and A. Iollo. Level-set, penalization and cartesian meshes: A paradigm for inverse problems and optimal design. *Journal of Computational Physics*, 228:6291–6315, 2009.
- [11] A. Chorin. A numerical method for solving incompressible viscous flow problems. *Journal of Computational Physics*, 135:115–125, 1997.
- [12] M. Cisternino and L. Weynans. A parallel second order cartesian method for elliptic interface problems. *Communications in Computational Physics*, 12(05):1562–1587, 2012.
- [13] A. Coco, G. Currenti, C. D. Negro, and G. Russo. A Second Order Finite-Difference Ghost-Point Method for Elasticity Problems on unbounded domains with applications to Volcanology. *Communications in Computational Physics*, 16:983–1009, 2014.
- [14] A. Coco and G. Russo. Second order multigrid methods for elliptic problems with discontinuous coefficients on an arbitrary interface, I: one dimensional problems. *Numerical Mathematics: Theory, Methods and Applications*, 5:19–42, 2012.

- [15] A. Coco and G. Russo. Finite-Difference Ghost-Point Multigrid Methods on Cartesian Grids for Elliptic Problems in Arbitrary Domains. *Journal of Computational Physics*, 241:464–501, 2013.
- [16] J. Dolbow and T. Belytschko. A finite element method for crack growth without remeshing. *International journal for numerical methods in engineering*, 46(1):131–150, 1999.
- [17] J. Dolbow and I. Harari. An efficient finite element method for embedded interface problems. *Int. J. for Num. Meth. in Eng.*, 78(229–252), 2009.
- [18] J. Donea. An arbitrary Lagrangian-Eulerian finite element method for transient fluid-structure interactions. *Computer Methods in Applied Mechanics and Engineering*, 33:689–723, 1982.
- [19] M. Dryja. A neumann-neumann algorithm for mortar discretization of elliptic problems with discontinuous coefficients. *Num. Math.*, 99(645–656), 2005.
- [20] A. du Chéné, C. Min, and F. Gibou. Second-Order Accurate Computation of Curvatures in a Level Set Framework Using Novel High Order Reinitialization Schemes. *Journal of Scientific Computing archive*, 35:114–131, 2008.
- [21] R. E. Ewing, Z. Li, T. Lin, and Y. Lin. The immersed finite volume element methods for the elliptic interface problems. *Mathematics and Computers in Simulation*, 50(1):63–76, 1999.
- [22] R. Fedkiw, T. Aslam, B. Merriman, and S. Osher. A Non-Oscillatory Eulerian Approach to Interfaces in Multimaterial Flows (The Ghost Fluid Method). *Journal of Computational Physics*, 152:457–492, 1999.
- [23] L. Formaggia and F. Nobile. Stability analysis of second-order time accurate schemes for ALE-FEM. *Computer Methods in Applied Mechanics and Engineering*, 193:4097–4116, 2004.
- [24] T.-P. Fries and T. Belytschko. The intrinsic xfem: a method for arbitrary discontinuities without additional unknowns. *International journal for numerical methods in engineering*, 68(13):1358–1385, 2006.
- [25] F. Gibou and R. Fedkiw. A second-order-accurate symmetric discretization of the poisson equation on irregular domains. *Journal of Computational Physics*, 176:205–227, 2002.
- [26] F. Gibou and R. Fedkiw. A fourth order accurate discretization for the laplace and heat equations on arbitrary domains, with applications to the stefan problem. *Journal of Computational Physics*, 202:577–601, 2005.
- [27] S. Groí and A. Reusken. An extended pressure finite element space for two-phase incompressible flows with surface tension. *Journal of Computational Physics*, 224(40–58), 2007.
- [28] A. Guittet, M. Lepilliez, S. Tanguy, and F. Gibou. Solving elliptic problems with discontinuities on irregular domains - the voronoi interface method. *Journal of Computational Physics*.
- [29] G. Guyomarc’h, C.-O. Lee, and K. Jeon. A discontinuous galerkin method for elliptic interface problems with application to electroporation. *Communications in numerical methods in engineering*, 25(10):991–1008, 2009.
- [30] W. Hackbusch. *Multi-grid methods and applications*. Springer, 1985.
- [31] A. Hansbo and P. Hansbo. A finite element method for the simulation of strong and weak discontinuities in solid mechanics. *Comput. Meth. in Appl. Mech. and Eng.*, 1993(3523–3540), 2004.
- [32] S. Hou, W. Wang, and L. Wang. Numerical method for solving matrix coefficient elliptic equation with sharp-edged interfaces. *Journal of Computational Physics*, 229:7162–7179, 2010.
- [33] J. Huang and J. Zou. A mortar element method for elliptic problems with discontinuous coefficients. *IMA J. Numer. Anal.*, 22(549–576), 2001.
- [34] J. J. E. Dendy. Black Box Multigrid. *Journal of Computational Physics*, 48:366–386, 1982.
- [35] H. Ji and J. Dolbow. On strategies for enforcing interfacial constraints and evaluating jump conditions with the extended finite element method. *International Journal for Numerical Methods in Engineering*, 61(14):2508–2535, 2004.

- [36] R. LeVeque and Z. Li. The immersed interface method for elliptic equations with discontinuous coefficients and singular sources. *SIAM J. Numer. Anal.*, 31:1019–1044, 1994.
- [37] A. J. Lew and G. C. Buscaglia. A discontinuous-galerkin-based immersed boundary method. *International Journal for Numerical Methods in Engineering*, 76(4):427–454, 2008.
- [38] Z. Li. A fast iterative algorithm for elliptic interface problems. *SIAM Journal of Numerical Analysis*, 35:230–254, 1998.
- [39] Z. Li and K. Ito. Maximum principle preserving schemes for interface problems with discontinuous coefficients. *SIAM Journal of Scientific Computing*, 23:339–361, 2001.
- [40] Z. Li and K. Ito. *The immersed interface method: numerical solutions of PDEs involving interfaces and irregular domains*. SIAM, 2006.
- [41] X. Liu, R. Fedkiw, and M. Kang. A Boundary Condition Capturing Method for Poissons Equation on Irregular Domains. *Journal of Computational Physics*, 160:151–178, 2000.
- [42] B. Lu, Y. Zhou, M. Holst, and J. McCammon. Recent progress in numerical methods for the poisson-boltzmann equation in biophysical applications. *Commun Comput Phys*, 3(5):973–1009, 2008.
- [43] A. Mayo. The fast solution of Poisson’s and the biharmonic equations on irregular regions. *SIAM J. Numer. Anal.*, 21:285–299, 1984.
- [44] C. Min and F. Gibou. A second order accurate projection method for the incompressible Navier-Stokes equations on non-graded adaptive grids. *J. Comput. Phys.*, 219:912–929, 2006.
- [45] Y. T. Ng, H. Chen, C. Min, and F. Gibou. Guidelines for Poisson solvers on irregular domains with Dirichlet boundary conditions using the ghost fluid method. *J. Sci. Comput.*, 41:300–320, 2009.
- [46] Y. T. Ng, C. Min, and F. Gibou. An efficient fluid-solid coupling algorithm for single-phase flows. *J. Comput. Phys.*, 228:8807–8829, 2009.
- [47] M. Oevermann and R. Klein. A Cartesian grid finite volume method for elliptic equations with variable coefficients and embedded interfaces. *Journal of Computational Physics*, 219:749–769, 2006.
- [48] M. Oevermann, C. Scharfenberg, and R. Klein. A sharp interface finite volume method for elliptic equations on Cartesian grids. *Journal of Computational Physics*, 228:5184–5206, 2009.
- [49] S. Osher and R. Fedkiw. *Level Set Methods and Dynamic Implicit Surfaces*. Springer-Verlag New York, Applied Mathematical Sciences, 2002.
- [50] J. Papac, F. Gibou, and C. Ratsch. Efficient Symmetric Discretization for the Poisson, Heat and Stefan-Type Problems with Robin Boundary Conditions. *Journal of Computational Physics*, 229:875–889, 2010.
- [51] C. S. Peskin. Numerical analysis of blood flow in the heart. *Journal of Computational Physics*, 25:220–252, 1977.
- [52] J. W. Ruge and Stüben. *Multigrid methods*, chapter Algebraic multigrid, pages 73–130. SIAM, Philadelphia, 1987.
- [53] G. Russo and P. Smereka. A remark on computing distance functions. *Journal of Computational Physics*, 163:51–67, 2000.
- [54] A. Sarthou, S. Vincent, J. Caltagirone, and P. Angot. Eulerian-Lagrangian grid coupling and penalty methods for the simulation of multiphase flows interacting with complex objects. *International Journal for Numerical Methods in Fluids*, 00:1–6, 2007.
- [55] M. Semplice, A. Coco, and G. Russo. Adaptive mesh refinement for hyperbolic systems based on third-order compact weno reconstruction. *Journal of Scientific Computing*, 66(2):692–724, 2016.
- [56] J. Sethian. *Level Set Methods and Fast Marching Methods: Evolving Interfaces in Computational Geometry, Fluid Mechanics, Computer Vision and Materials Science*. Cambridge University Press, 1999.

- [57] M. Sussman, P. Smereka, and S. Osher. A level set approach for computing solutions to incompressible 2-phase flow. *Journal of Computational Physics*, 114:146–159, 1994.
- [58] M. Sussman, K. M. Smith, M. Y. Hussaini, M. Ohta, and R. Zhi-Wei. A sharp interface method for incompressible two-phase flows. *Journal of computational physics*, 221(2):469–505, 2007.
- [59] U. Trottenberg, C. Oosterlee, and A. Schuller. *Multigrid*. Academic Press, 2001.
- [60] J. W. L. Wan and X.-D. Liu. A boundary condition-capturing multigrid approach to irregular boundary problems. *Journal of Scientific Computing*, 25:1982–2003, 2004.
- [61] W. L. Wan. Interface preserving coarsening multigrid for elliptic problems with highly discontinuous coefficients. *Numer. Linear Algebra Appl.*, 7:727–741, 2000.
- [62] Y. Yang and H. Udaykumar. Sharp interface cartesian grid method iii: Solidification of pure materials and binary solutions. *Journal of Computational Physics*, 210(1):55–74, 2005.
- [63] S. Yu, Y. Zhou, and G. Wei. Matched Interface and Boundary (MIB) method for elliptic problems with sharp-edged interfaces. *Journal of Computational Physics*, 224:729–756, 2007.

**LaTeX Source Files**

[Click here to download LaTeX Source Files: JCP\\_submission.zip](#)